Single-step growth of graphene and graphene-based nanostructures by plasma-enhanced chemical vapour deposition

IOP Publishing Nanotechnology
Nanotechnology **XX** (XXXX) XXXXXX https://doi.org/XXXX/XXXX

Single-step growth of graphene and graphene-based nanostructures by plasma-enhanced chemical vapour deposition

Nai-Chang Yeh[1,2], Chen-Chih Hsu[1], Jacob Bagley[3], and Wei-Shiuan Tseng[1]

[1] Department of Physics, California Institute of Technology, Pasadena, California 91125, USA
[2] Kavli Nanoscience Institute, California Institute of Technology, Pasadena, California 91125, USA
[3] Department of Chemistry, California Institute of Technology, Pasadena, California 91125, USA

E-mail: ncyeh@caltech.edu

Received xxxxxx
Accepted for publication xxxxxx
Published xxxxxx

Abstract

The realization of many promising technological applications of graphene and graphene-based nanostructures depends on the availability of reliable, scalable, high-yield and low-cost synthesis methods. Plasma enhanced chemical vapor deposition (PECVD) has been a versatile technique for synthesizing many carbon-based materials, because PECVD provides a rich chemical environment, including a mixture of radicals, molecules and ions from hydrocarbon precursors, which enables graphene growth on a variety of material surfaces at lower temperatures and faster growth than typical thermal chemical vapor deposition (T-CVD). Here we review recent advances in the PECVD techniques for synthesis of various graphene and graphene-based nanostructures, including horizontal growth of monolayer and multilayer graphene sheets, vertical growth of graphene nanostructures (VG-GNs) such as graphene nanostripes (GNSPs) with large aspect ratios, direct and selective deposition of monolayer and multi-layer graphene on nanostructured substrates, and growth of multi-wall carbon nanotubes (MWCNTs). By properly controlling the gas environment of the plasma, it is found that no active heating is necessary for the PECVD growth processes, and that high-yield growth can take place in a single step on a variety of surfaces, including metallic, semiconducting and insulating materials. Phenomenological understanding of the growth mechanisms are described. Finally, challenges and promising outlook for further development in the PECVD techniques for graphene-based applications are discussed.

Keywords: graphene, vertically grown graphene nanostructures (VG-GNs), graphene nanostripes (GNSPs), carbon nanotubes (CNTs), plasma enhanced chemical vapour deposition (PECVD), thermal chemical vapour deposition (T-CVD)

1. Introduction – A new era of graphene-based technologies

Graphene, a single layer of carbon atoms forming a honeycomb lattice structure with two-dimensional sp^2 bonding, has simulated intense research activities since its experimental isolation in 2005 because of its superior and novel electronic, optical, thermal, magnetic and mechanical properties that are promising for a wide range of technological applications [1-4]. Despite abundant scientific advances and prototype device demonstrations mostly based on small pieces of mechanically exfoliated graphene, the full potential of graphene-based technologies in such large-scale

applications as in supercapacitors and lithium-ion batteries for energy storage, in photovoltaic and fuel cells for energy conversion and in large panels for display cannot be realized unless high-quality graphene can be reliably synthesized in mass quantities and at low costs. On the other hand, compatibility of the graphene growth process with CMOS technologies will be critical to the realization of graphene-based nanoelectronic and optoelectronic applications. Moreover, efficient and scalable graphene transfer technologies from their growth substrates to desirable targets without degrading the sample quality will be necessary for many industrial applications. These technical challenges place strong constraints on the methods of graphene production. The purpose of this review is to provide an update on recent advances in the graphene growth technologies based on plasma-enhanced chemical vapour deposition (PECVD), including the growth of graphene sheets and graphene-based nanostructures on different substrates, as well as the selective growth of graphene on nanostructures in real industrial semiconductor wafers, and then presents an outlook for the promises and challenges ahead to advance the research and technology.

1.1. Current techniques used for synthesis of graphene and graphene-based nanostructures

To date several methods have been developed for mass-production of graphene, which include liquid-phase exfoliation of graphite [5, 6], synthesis on SiC [7, 8], thermal chemical vapour deposition (T-CVD) [9], and plasma-enhanced chemical vapour deposition (PECVD) [10, 11]. Among these different synthesis methods, T-CVD has been developed for growing large-area graphene with reasonably high quality. However, T-CVD growth of graphene generally requires multiple processing steps and relatively long time in both substrate preparation and graphene growth [12-14]. Moreover, high-temperature processes (~ 1000 °C) in the T-CVD synthesis are incompatible with applications relevant to semiconducting industry, and the high thermal budget adds further constraints on mass production. Recently, oxygen and oxygen containing species were also found to play an important role in graphene synthesis, such as graphene nucleation, graphene shape, and bilayer and multilayer graphene formation [12, 15-17].

In contrast to the T-CVD growth method, PECVD has proven to be a versatile approach that offers a number of advantages [10, 11]. PECVD has been widely used for synthesizing many carbon-based materials, such as diamonds, graphene, vertically oriented graphene nano-walls and nano-sheets, and carbon nanotubes (CNTs). The plasma can provide a rich chemical environment, including a mixture of free radicals, photons, energetic electrons, excited molecules and active ions. This environment enables graphene growth on different surfaces at relatively lower temperatures and faster growth than T-CVD [10, 11]. Additionally, PECVD techniques can be employed for fast and large-scale functionalization of graphene and related materials, which is a versatile approach that further broadens the scope of graphene-based applications. These advantages make PECVD growth of graphene and graphene-related nanostructures highly attractive, and have been considered as a promising technique to improve the compatibility of graphene growth with semiconducting manufacturing processes.

1.2. Plasma sources for PECVD growth techniques

Before we proceed further with the PECVD conditions for graphene synthesis, it is informative to briefly summarize typical plasma sources used in PECVD processes. Different plasma sources can be categorized by different power frequencies, which include: direct current (DC) gas discharge sources; radio frequencies (RF) sources with frequencies ranging from 1 to 500 MHz; microwave (MW) sources with frequencies ranging from 0.5 to 10 GHz; and combinations of the aforementioned types.

Typical DC-PECVD synthesis involves a relatively simple setup using the parallel-plate dc glow discharge. With a sufficient potential applied between the planar cathode and anode, Townsend breakdown will occur and plasma is generated [10]. The RF sources have three main modes for coupling the energy of an RF generator to the plasma: the evanescent electromagnetic (H) mode, the propagating wave (W) mode, and the electrostatic (E) mode [10]. The MW sources typically operate with either the transverse magnetic (TM) or transverse electric (TE) propagation modes [10]. The choice of the plasma source and reactor configuration for PECVD growth of graphene depends on the specific applications and the growth substrates. Among different plasma sources and reactor configurations, the most efficient delivery of power per unit volume is the TM-MW frequencies. On the other hand, in the event of delicate substrates or specific applications that are sensitive to ionic bombardment and/or ultraviolet (UV) light exposure, configurations with remote plasma arrangements may become desirable. A recent review by Z. Bo *et al.* [10] contains comprehensive accounts and references for various plasma sources and reactor configurations that are employed for PECVD growth of graphene nanostructures, and so we shall not elaborate different techniques further here. In the following we shall simply specify the PECVD method used when we compare the growth conditions and the resulting graphene characteristics by various research groups.

1.3. Outline of this review

The remaining part of this article is structured as follows. Section 2 is devoted to the status of horizontal growth of large-area graphene sheets and selective growth of graphene

on nanostructures by PECVD, studies of the resulting graphene characteristics, and discussions of their potential applications. Section 3 describes high-yield vertical growth of graphene nanostructures, including quasi-one dimensional graphene nanostripes (GNSPs) by seeded PECVD methods, and the studies of their properties. In Section 4 recent progress in the vertical growth of multi-wall carbon nanotubes (CNTs) on different substrates by PECVD is reviewed. In Section 5 we discuss important issues associated with further development of PECVD and related techniques for graphene-based applications. Finally we summarize in Section 6 the status of PECVD growth of graphene and graphene based nanostructures, and present an outlook for new directions and challenges.

2. PECVD growth of graphene on different substrates

In this section, we review recent progress in PECVD growth of graphene sheets on different substrates and selective horizontal growth of multilayer graphene on nanostructures of real industrial semiconductor wafers.

2.1. Reviews of PECVD growth of graphene

2.1.1 PECVD growth of graphene sheets on transition metal substrates

Generally speaking, graphene growth could be achieved at a reduced temperature by PECVD on different transition metal substrates such as Co [18, 19], Ni [20-23], and Cu [11, 24-31]. Among the pioneering works, Woo *et al.* grew high-quality and uniform graphene films at 850 °C in a remote radio frequency PECVD (RF-PECVD) system [20]. SEM images and electron backscattering diffraction map showed highly crystallized graphene with few atomic defects and well-ordered structure. The carrier mobility was ~ 4500 $cm^2V^{-1}s^{-1}$ at room temperature. Nandamuri *et al.* also employed a RF-PECVD system to synthesize multilayer graphene (MLG) on Ni (111) single crystals and polycrystalline Ni foils in about one-minute growth time [21]. The size of the graphene domains was found to be consistent with the dimensions of the flat grain Ni surfaces, which ranged from ~ 1 μm to ~ 20 μm, suggesting epitaxial growth on the Ni polycrystalline substrate. Subsequently, single layer graphene (SLG) was successfully grown on Ni foil by MW-PECVD with the growth temperature from 450 to 750 °C [22], and the number of graphene layers could also be controlled by changing the gas mixture of H_2/CH_4 ratio. Peng *et al.* demonstrated the synthesis of few-layer graphene sheets on an ultra-thin Ni film coated on SiO_2/Si substrate using low temperature RF-PECVD without introducing any H_2 [23], where the number of graphene layers could be controlled by the thickness of Ni film at 475 °C. In general, it is found that the use of Ni substrates for graphene synthesis by PECVD methods typically yields MLG due to the high carbon solubility in Ni, similar to the findings in T-CVD graphene growth.

On the other hand, Cu foils have been widely used for graphene growth because of the low cost and commercial availability. Moreover, Cu is an excellent substrate for synthesizing high quality monolayer graphene due to the low carbon solubility and its catalytic nature. With the help of plasma, hydrocarbon precursors can break apart more easily so that carbon atoms and radicals can directly assemble into graphene on the Cu surface. For example, Kim *et al.* have deposited large-area graphene-like films on Al and Cu foils using a microwave assisted surface wave plasma CVD (MW-SWP-PECVD) method at a substrate temperature ~ 400 °C [24]. However, graphene films grown by MW-SWP-PECVD required high power (3 to 4.5 kW), and their Raman spectroscopy exhibited large *D* and *D′* peaks, which indicated lots of defects and boundaries. Similarly, Terasawa *et al.* investigated the growth mechanism of graphene in varying the growth conditions by a RF-PECVD [25]. When the substrate temperature was kept at 500 °C, carbon nano-walls (CNWs) were found on the Cu surface. On the other hand, as the substrate temperature was raised to 900 °C, SLG was fabricated with a small *D* peak. It was found that the growth of SLG was activated by the Cu catalytic surface at high substrate temperature, whereas the growth of CNWs was initiated by the hydrocarbon radicals in the plasma.

In the following years, the growth of graphene based on PECVD methods faced two major challenges. One was to fabricate continuous and large areas of graphene films, and the other was to improve the quality of the PECVD-grown graphene. Yamada *et al*. combined a PECVD process at a low substrate temperature of ~ 380 °C and a roll-to-roll process for mass production of graphene [26]. Although the resulting graphene structures were defective, Raman spectra along the width direction of the Cu foil was found to be uniform. This result suggested that roll-to-roll growth by the PECVD method appeared promising for realizing continuous and large area graphene films in industrial production.

Meanwhile, many research groups have experimented different PECVD systems and growth conditions to improve the quality of graphene grown on Cu substrates. Kim *et al*. demonstrated synthesis of SLG on polycrystalline Cu foils under various Ar/CH_4 and H_2/CH_4 gas ratios for substrate temperatures ranging from 700 °C to 830 °C [27]. The grain size of graphene was found to range from ~ 0.4 to ~ 3 μm and the shape was arbitrary or rounded hexagonal. In particular, they found out even without any H_2 flow, methane alone could still provide enough hydrogen species for single-layer graphene synthesis on Cu by PECVD, which implied that methane could be the source for both hydrogen and carbon. Similar graphene films were synthesized using remote MW-PECVD at substrate temperature of 600 °C with

various ratios of methane and hydrogen mixture [28]. The remote plasma setup used in the work could reduce defects incurred from ion bombardment in the plasma. Moreover, it was found that with increasing H_2 flow rate, Raman spectra showed higher-quality graphene films with larger 2*D*-to-*G* and smaller *D*-to-*G* intensity ratios as well as narrower FWHMs of the 2*D* band. Nang *et al.* also demonstrated graphene synthesis on Cu foils by means of inductively-coupled plasma chemical vapour deposition (ICPCVD) [30]. Graphene quality was found to improve with increasing growth time and plasma power. In 2015, Laan *et al.* used RF-PECVD to grow SLG at substrate temperatures as low as 220 °C [31]. These graphene films could be easily removed from Cu foils and transferred to other substrates by dipping the sample into water. Recently, Boyd *et al.* [11] demonstrated a single-step process to grow graphene by MW-PECVD without any active heating of the substrates. The graphene sheets were almost strain free and the mobility was as high as >~ 60, 000 cm^2/V-s at 300 K.

In Table 1 we summarize the aforementioned PECVD growth conditions on metallic substrates and the resulting graphene characteristics from measurements of Raman spectroscopy, sheet resistance and electrical mobility. Here we note that Raman spectroscopy has been a powerful experimental tool that can reveal numerous important characteristics of graphene samples [32]. As detailed in Refs. [32,33], Raman spectroscopic studies of graphitic samples can provide useful information about the number of layers, stacking order, disorder, as well as the behaviour of electrons and phonons in the samples. The most prominent features in the Raman spectra of monolayer graphene include the so-called *G*-band appearing at ~ 1582 cm^{-1} and the 2*D* (also known as *G*′) band at ~ 2700 cm^{-1}, using laser excitation at 2.41 eV. In the case of a disordered sample or at the edge of a graphene sample, the so-called disorder-induced *D*-band at around ~ 1350 cm^{-1} is also present. The *G*-band is a first-order Raman process associated with the doubly degenerate (in-plane transverse optical and longitudinal optical) phonon mode (E_{2g} symmetry) at the centre of the Brillouin zone. The *D*-band is a second-order Raman process involving one in-plane transverse optical phonon and a defect mode due to imperfections such as defects, edges and folds. The 2*D*-band corresponds to a second-order Raman process that involves two in-plane transverse phonon modes, which is a mode of particular interest for analysing the number of graphene layers and stacking order in multilayer graphene based on its linewidth and peak position [32]. For instance, the 2*D*-band of bilayer graphene with perfect Bernal A-B stacking should be considered as the superposition of four Lorentzian peaks that correspond to four different double resonance processes associated with bilayer graphene, whereas that of trilayer graphene with A-B-A stacking would involve six Lorentzian peaks [32]. In the case of perfect 3D graphite, the 2*D*-band consists of two Lorentzian peaks, whereas for randomly oriented, turbostratic multilayer graphene layers, the 2*D*-band appears as a single Lorentzian like that in monolayer graphene but with a larger linewidth [32]. Additionally, the biaxial strain ($\varepsilon_{ll} + \varepsilon_{tt}$) associated with monolayer graphene can be estimated by considering the Raman frequency shifts $\Delta\omega \equiv \left(\omega_{\mathrm{m}} - \omega_{\mathrm{m}}^{0}\right)$ and the Grüneisen parameter $\gamma_{\mathrm{m}}^{\mathrm{biax}}$ [33]:

$$\gamma_{\mathrm{m}}^{\mathrm{biax}} = \frac{\Delta\omega_{\mathrm{m}}}{\omega_{\mathrm{m}}^{0}\left(\varepsilon_{ll} + \varepsilon_{tt}\right)}, \quad (1)$$

where m (= *G*, 2*D*) refers to the specific Raman mode, and ω_{m}^{0} is the corresponding resonant frequency in the absence of strain. Furthermore, for polycrystalline graphene samples, the average in-plane sp^2 crystallite size (L_a) of the samples may be estimated by using the intensity ratio (I_D / I_G) [34]:

$$L_a\left(\mathrm{nm}\right) = \frac{560}{E_L^4}\left(\frac{I_D}{I_G}\right)^{-1}, \quad (2)$$

where E_L denotes the excitation energy of the laser source. Therefore, a variety of useful information about the quality and structural characteristics of graphene samples can be obtained by analyzing the peak frequencies, linewidths and relative intensities of prominent Raman modes.

2.1.2 PECVD graphene on non-metal substrates

The rich radical environment provided by PECVD has also been exploited to synthesize graphene on non-metallic substrates. In particular, direct growth of graphene on semiconducting substrates (such as Si and Ge) and dielectric substrates (such as SiO_2 and HfO_2) is technologically very important for better integration of graphene into current semiconductor industry [35, 36]. Moreover, direct growth of graphene on desirable non-metallic substrates eliminates the need of transferring samples from their growth substrates, preventing potential degradation of sample quality during the transfer process. By using precursors such as CH_4, C_2H_2, H_2, and CO_2, direct growth of graphene has been demonstrated on semiconducting substrates of Ge [37-40] and Si [41-44], and on dielectric substrates of GaN [45, 46], SiC [44, 47], SiO_2 [48-51], hexagonal boron nitride (*h*-BN) [52], Al_2O_3, sapphire, quartz, mica, and even 4-inch glass wafers [53, 54].

On Ge, growth of high-quality graphene with large and uniform areas (up to centimeters) had been achieved [39]. On the other hand, for graphene growth on Si or SiO_2 substrates, the inert silicon surface makes the nucleation and deposition of graphene very difficult to happen. To date, it is still challenging to directly synthesize large area, flat graphene sheets on silicon without using any metal catalysts. Given the reactive radicals inside the plasma cavity, PECVD growth could be a good solution that provides a better environment

for anchoring carbon and also higher energy for reactions to take place as compared with thermal CVD systems. However, it was found that metal-assisted growth was often needed in the PECVD growth, because without any transition metal catalysts, graphene tended to stop growth quickly after initial nucleation and the resulting sample often contained many structural defects, forming networked nano-graphite [41], island type nano-graphene [42], or graphene nano-walls [43]. For instance, Kim *et al.* used a remote Cu catalyst method by putting a Cu foil on top of a SiO_2 substrate [51]. On the other hand, continuous SLG sheets could be grown between a thin Ni film and a SiO_2 interface. The carrier mobility ranged from 43 to 580 cm^2/V-s, which was almost on the same order as that of the graphene directly fabricated on the SiO_2 substrate by thermal CVD.

In contrast to catalysing graphene growth by transition metals, Wei *et al.* found a critical equilibrium state between H_2 plasma etching and CH_4 or C_2H_4 plasma CVD [55], which led to the growth of micrometer-scale graphene directly on sapphire, HOPG, and SiO_2 substrates at temperatures as low as 400 °C. However, the growth process described by Wei *et al.* [55] required preparation of seeds on the substrates first, which was followed by multiple synthesis steps, suggesting the generic difficulties in direct growth of graphene on non-metallic substrates. Similarly, Kato *et al.* developed a method for growing graphene directly on a SiO_2 substrate by rapid-heating plasma CVD so as to provide sufficient energy [56].

Hexagonal boron nitride (*h*-BN) is a wide bandgap insulator known to be an ideal substrate for graphene because of its atomically flat surface, small lattice mismatch to graphene and the ability to tune graphene electronic structure [57-60]. Therefore, it is highly desirable to experiment direct PECVD growth of graphene on *h*-BN. In 2013, Yang *et al.* reported epitaxial growth of single-domain graphene on *h*-BN by a plasma-assisted deposition method [52], and found that the growth of continuous single-crystalline SLG or bilayer graphene films was only limited by the size of the *h*-BN substrates.

Gallium nitride (GaN) is a binary III/V direct bandgap semiconductor commonly used for applications in various optoelectronic, high-power and high-frequency devices. Sun *et al.* first attempted direct growth of graphene on the surface of the GaN (0001)/sapphire substrate by T-CVD at 950°C under a high flow of ammonia without metallic catalysts [45]. They found that the synthesized carbon thin films were largely sp^2 bonded, macroscopically uniform, NS electrically conducting, with optical transparencies comparable to that of exfoliated graphene [45]. Subsequently, Kim *et al.* demonstrated plasma-assisted direct synthesis of graphene films on GaN substrates [46], and found that the active layer in the light emitting diode (LED) was not degraded by the growth temperature of graphene so that the deposited graphene could act as a transparent conducting electrode without the need of any transfer process.

While progress has been made in the PECVD growth of graphene on non-metallic substrates, it is clear that much more effort is still needed to establish the growth conditions for synthesizing high-quality large-area graphene on a wide variety of dielectric and semiconducting surfaces.

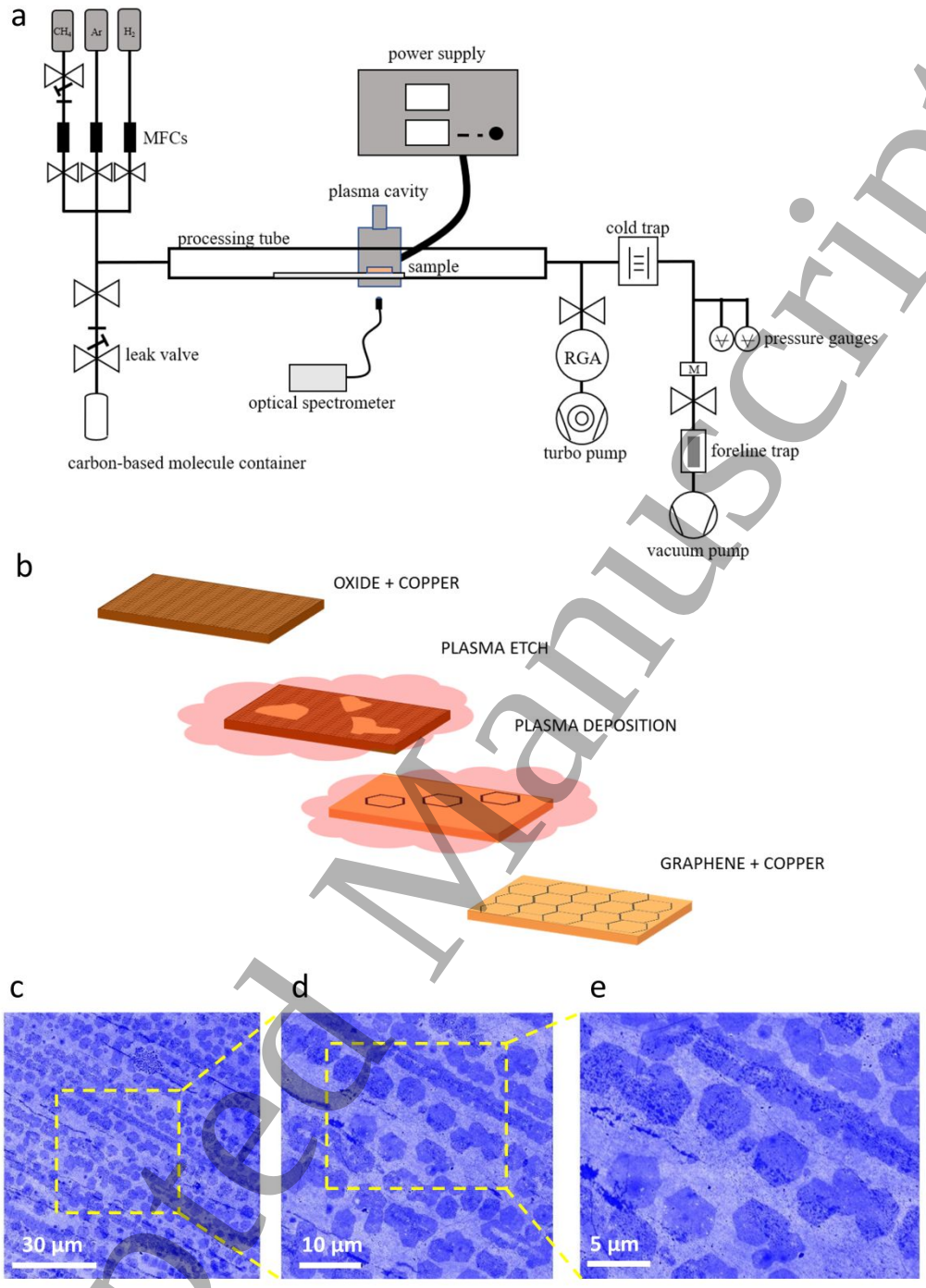

Figure 2.1 (a) A schematic of the PECVD setup for synthesis of graphene sheets and VG-GNs without active heating. Adapted from Ref. [11]. (b) Schematic illustration of the single-step PECVD growth mechanism of graphene on copper. (c-e) False-color SEM images of graphene grown for excessive time and transferred to single crystalline sapphire, with increasing magnification from left to right, showing well-aligned, hexagonal adlayer graphene domains (dark) on the bottom monolayer graphene (light), which illustrate how the hexagonal grains nucleated along parallel lines of the copper foil coalesce into a single sheet of graphene.

Table 1. Comparison of different synthesis conditions for PECVD-growth of monolayer graphene on metallic substrates and the resulting characteristics of the graphene samples. Here RT refers to room temperature.

Method	Material	Growth Time	Growth Temp. (°C)	I_{2D}/I_G	I_D/I_G	$FWHM_{2D}$ (cm^{-1})	Grain Size	Sheet Resistance (Ω/sq)	Mobility ($cm^2V^{-1}s^{-1}$)	Ref
RF-PECVD	Co	15 s ~ 20 min	800	1.25 ~ 1.75	0.35~ 0.68	73 ~ 80	22 ~ 63 nm	–	–	18
RF-PECVD	Co	40 s	800	< 1	0.131	–	–	2661	–	19
RF-PECVD	Ni	5 min	850	0.71 ~ 2.03	~ 0	–	tens of μm	–	4500 (@RT)	20
RF-PECVD	Ni	1 min	650 ~ 700	0.24	~ 0	–	< 1 μm ~ 20 μm	–	3000	21
MW-PECVD	Ni	1 min	450 ~ 750	0.6 ~ 3.7	0.01 ~ 0.5	29 ~ 46	–	590 ~ 1855	–	22
RF-PECVD	Ni	100 ~ 600 s	475	0.22 ~ 1	0.2 ~ 1.8	33 ~ 60	–	4226 ~ 9142	–	23
MW-SWP-PECVD	Cu, Al	30 ~ 180 s	300 ~ 400	3.4	2.52	37	< 1 μm	1000 ~ 4100	–	24
RF-PECVD	Cu	5 min	950	0.2 ~ 2.25	1 ~ 1.5	–	10 ~ 20 nm	–	–	25
MW-SWP-PECVD	Cu	96 s	380	0.12 ~ 0.85	1.1 ~ 2.19	–	5 ~ 15 nm	9×10^5 ~ 3×10^6	–	26
RF-PECVD	Cu	0.2 ~ 4 min	700 ~ 830	2.2 ~ 4	0.2 ~ 0.7	31 ~ 43	0.4 ~ 3 μm	–	3200 (@RT)	27
MW-SWP-PECVD	Cu	2 ~ 4 min	240 ~ 500	0.42 ~ 0.78	1.39 ~ 2.25	–	–	10030	–	28
DC-PECVD	Cu	5 min	600	0.98 ~ 2.29	0.13 ~ 0.33	35 ~ 39	–	–	–	29
RF-PECVD	Cu	5 s ~ 60 min	950	0.98	0.11 ~ 0.82	–	–	1950 ~ 5200	–	30
RF-PECVD	Cu	2 and 4 min	220	1.51 ~ 1.72	0.78	–	0.1 ~ 1.2 μm	800	200	31
MW-PECVD	Cu	5 ~ 20 min	420	2.7	~ 0	28.8	a few mm's	–	3×10^4 ~ 6×10^4 (@RT)	11

2.2. Single-step deposition of high-mobility graphene at reduced temperatures

We have recently developed a new growth method based on MW-PECVD under no active heating to the substrates [11, 61]. This new method has been shown to reproducibly achieve, in one step, high-mobility large-sheet graphene samples that are nearly strain free [11].

The PECVD system is schematically illustrated in Figure 2.1(a). It consists an Evenson cavity and a power supply (MPG-4, Opthos Instruments Inc.), which provides an exciting MW frequency of 2.45 MHz to generate plasma. A residual gas analyzer (RGA) is used to monitor the precursor and by-products partial pressure. The gas delivery system consists of mass flow controllers (MFCs) for H_2, CH_4 and Ar. The CH_4 gas flow is controlled by a leak valve placed before the methane MFC. Other than these typical gases to grow large-area graphene sheets, a quartz container stored with some substituted aromatics may be attached to the growth chamber via a leak valve and a quarter-turn, shut-off valve. With the addition of substituted aromatics such as 1,2-dicholorobenzene (1,2-DCB), 1,2-dibromobenzene(1,2-DBB), 1,8-dibromonaphthalene (1,8-DBN) and toluene as the seeding molecules, we can choose to grow graphene nanostripes (GNSPs) [61] and carbon nanotubes (CNTs) vertically, which will be elaborated later in Sections 3 and 4.

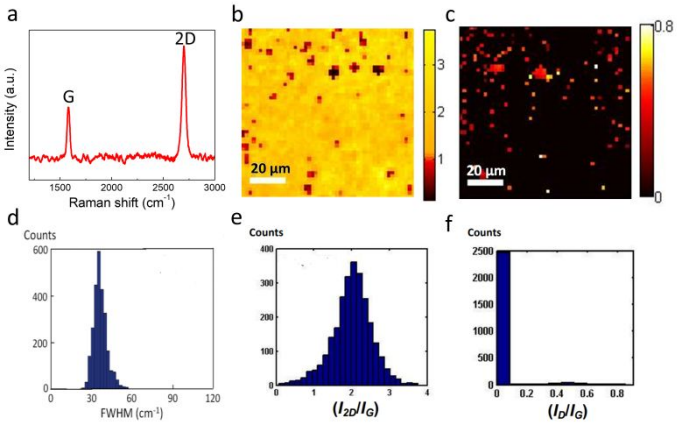

Figure 2.2 Raman spectroscopic characterizations of monolayer graphene samples grown by the single-step PECVD process [11]: (a) A representative point Raman spectrum of the PECVD-grown graphene taken at laser wavelength at 532 nm. (b) A spatial map for the intensity ratio of the 2D-to-G modes over an area of (100 × 100) μm^2 with the spectra were taken at 2 mm per pixel steps. (c) A spatial map for the intensity ratio of the D-to-G modes over the same (100 × 100) μm^2 area as shown in (b). (d) Histogram of the FWHM of the 2D mode taken over the same (100 × 100) μm^2 area as shown in (b) and (c). (e) Histogram of the intensity ratios of 2D-to-G modes, (I_{2D}/I_G), as shown in (b). (f) Histogram of the intensity ratios of D-to-G modes, (I_D/I_G), as shown in (c).

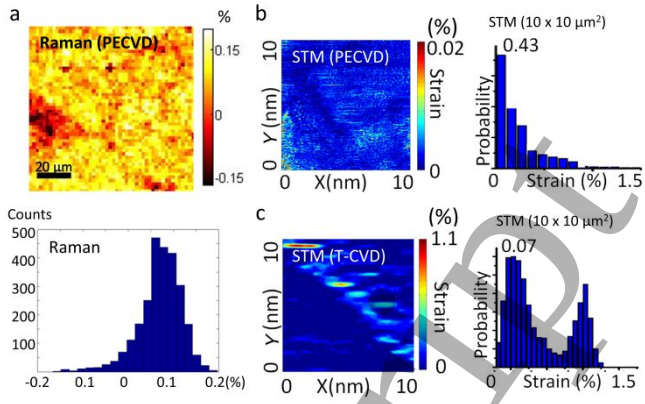

Figure 2.3 Comparison of the strain in as-grown monolayer graphene samples on Cu by PECVD and T-CVD methods [11]: (a) Strain map (upper panel) and the corresponding histogram (lower panel) of PECVD-grown graphene over a (100 × 100) μm^2 area as derived from Raman spectroscopic studies. (b) Strain map (left panel) and the corresponding histogram (right panel) of PECVD-grown graphene over a (10 × 10) nm^2 area as derived from STM topographic studies. (c) Strain map (left panel) and the corresponding histogram (right panel) of T-CVD grown graphene over a (10 × 10) nm^2 area as derived from STM topographic studies.

In this new approach, cyano radicals play an important role in a hydrogen-methane plasma to remove Cu native oxide without active heating. After Cu is smoothly etched, graphene growth is found to nucleate from arrays of well-aligned hexagonal domains and eventually coalesced into a large sheet of ~ 1 cm^2, as schematically shown in Figure 2.1(b) and further exemplified in Figure 2.1(c)-(e) [11]. Detailed Raman spectroscopic studies of these SLG graphene sheets generally revealed excellent spectral quality, as exemplified by a typical point spectrum in Figure 2.2(a), and maps as well as the corresponding histograms of the 2*D*-to-*G* and *D*-to-*G* intensity ratios over a (100 × 100) μm^2 area of a graphene sample on Cu foil in Figures 2.2(b) and 2.2(c), respectively. Clearly the samples are mostly SLG with few defects, as further manifested in Figures 2.2(d)-(e) by the histograms of the FWHM of the 2*D* mode, and the intensity ratios of the 2*D*-to-*G* and *D*-to-*G* modes, (I_{2D}/I_G) and (I_D/I_G), respectively.

Moreover, estimates of the magnitude of strain from both Raman spectroscopy and scanning tunnelling microscopy (STM) [11] revealed that the spatial strain distribution in the PECVD-grown graphene, as exemplified in Figure 2.3(a) for the biaxial strain determined from the Raman spectroscopic studies using Equation (1) and in Figures 2.3(b) and 2.3(c) for strain derived from atomically resolved STM topographic studies [11], is nearly strain-free with an average of <~ 0.07% strain. The average strain in PECVD-grown graphene was consistently more than one order of magnitude smaller than that of the SLG grown by the T-CVD method, as exemplified by the strain maps shown in Figures 2.3(b) and 2.3(c). The finding of much reduced strain in our PECVD-grown graphene samples is also consistent with their much better electrical mobility, typically 30,000 ~ 70,000 cm^2/V-s at 300 K, which is comparable to the best values (40,000 ~ 60,000 cm^2/V-s) reported in multi-step, thermal CVD-grown single crystalline graphene at 1.7 K [12].

In addition to the high electrical mobility, we note that large-area strain-free graphene may be applied to *strain engineering* of novel nano-electronics by transferring strain-free monolayer graphene to substrates with pre-designed nanostructures to induce controlled spatial distributions of strain [62]. This approach is achievable because the local electronic properties of graphene are known to be highly susceptible to nanoscale lattice distortions [62 - 65]. Thus, proper design of the strain induced on graphene by its underlying, nanoscale architected substrates can result in desirable modifications to the local electronic properties of graphene [62]. Such nanoscale strain engineering of graphene for novel electronics [62] is only feasible with the availability of sizable and nearly strain-free graphene

synthesized by the PECVD method described in Reference [11].

2.3. Selective growth of PECVD graphene on Cu nanostructures

The impermeability [66] and oxidation resistance [67] of graphene makes it an ideal candidate as a protection barrier material for Cu interconnects to prevent oxidation and diffusion of Cu into the underlying low-k dielectrics. Kang *et al.* [68] synthesized graphene on Cu conducting lines of 2 μm width by the T-CVD method, and found that the resistance was reduced by 2%–7% and the breakdown current density was increased by 18% compared to pure Cu wires. Mehta *et al.* [69, 70] investigated low temperature (~650 °C) deposition of graphene around Cu nanowires, and found that the graphene deposition enhanced both the electrical and thermal conductivity. They also demonstrated successful blockage of Cu ion diffusion by large area multi-layer graphene membranes deposited directly on silicon oxide using PECVD. However, these experimental studies all involved high temperature synthesis of graphene (> 550 °C), which was incompatible with typical CMOS processing temperatures (< 450 °C). Further, none of the aforementioned studies were carried out on realistic industrial wafers with high-density nanostructures on delicate low-k dielectrics.

We have recently demonstrated the feasibility of growing graphene selectively on nanoscale Cu-interconnects in realistic industrial semiconductor wafers by a single-step PECVD technique and have further optimized the processes to minimize plasma-induced damages to the underlying low-k dielectrics. Our substrates were fabricated by an industrial semiconducting company. As shown in Figure 2.4(a), SEM images with increasing magnification show micro-sized Cu pads (middle image) and Cu nanostructures with different widths (right image). The bright areas in the SEM images represented Cu coated device and interconnect structures, and the dark areas represented a low k dielectric material. Using proper growth conditions, we could reproducibly deposit high-quality and continuous graphene layers onto the Cu nanostructures in the industrial wafers. Moreover, the low plasma power density (10 W for ~ 1 cm^3 volume) employed in the PECVD growth corresponded a gas temperature < ~ 100 °C, which was fully compatible with the current fabrication processes in semiconducting industry.

However, the PECVD process was found to induce some damages to the low-k dielectrics, depending on the growth parameters and schemes of experimental setups. The damages induced by plasma to the low-k dielectrics were mainly due to ion bombardment and UV light, as schematically shown in the left panel of Figure 2.4(b). In Figures 2.4(c) and 2.4(d) we show the AFM images of the region indicated by the blue box in Figure 2.4(a) after graphene growth. In Figure 2.4 (c) for graphene grown under direct exposure to plasma, many clusters appeared on the surface due to the low-k material etched by plasma and redeposited on the Cu surface and the graphene structures grown on Cu appeared inhomogeneous. To mitigate the plasma induced damages to the low-k dielectrics, we introduced a holed HOPG plate as a UV absorber, as

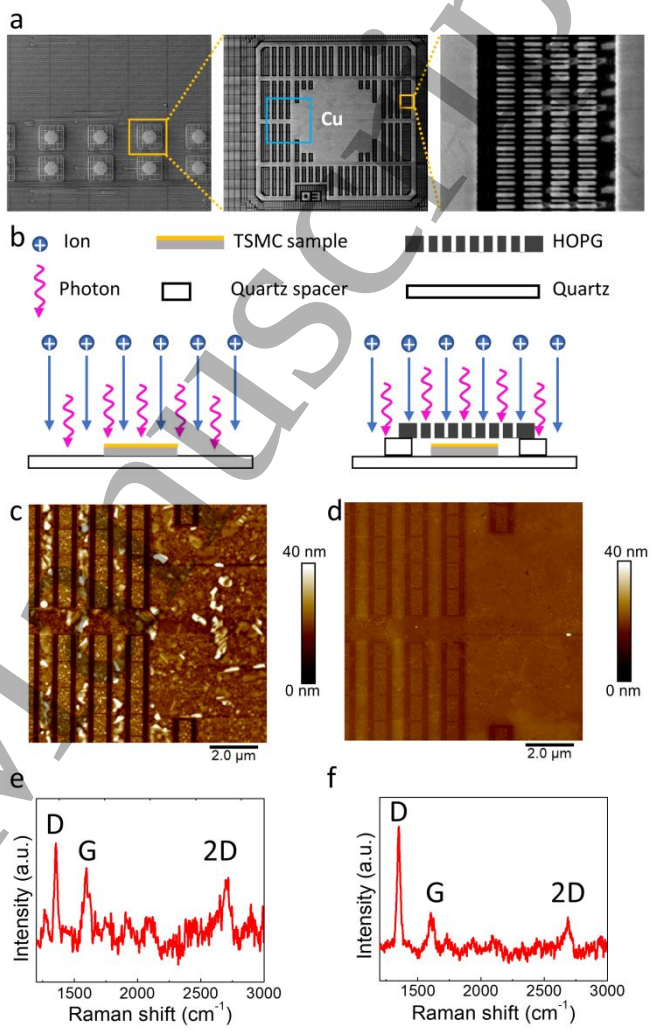

Figure 2.4 (a) SEM images of industrial wafers with increasing magnification (by ×10 from the left to the middle and by ×20 from the middle to the right). Right image shows Cu nanostructures with different widths, and the smallest features are <~ 20 nm. (b) Schematic drawings of the side view for the direct PECVD growth configuration (left) and that for the PECVD growth configuration with a holed HOPG plate as the UV absorber (right). (c) & (d) AFM images corresponding to the region indicated by the blue box in (a), after direct PECVD growth (left) and growth with HOPG absorber (right), respectively. (e) & (f) Raman spectra of (c) and (d), respectively.

schematically shown in the right panel in the Figure 2.4 (b). Using this configuration, we were able to block most of the UV light and minimize damages to the low-k dielectrics. AFM images taken after graphene growth with the HOPG UV absorber as shown in Figure 2.4 (d) revealed significant improvement on the surface and better Raman spectra (Figures 2.4 (e) and 2.4 (f)).

3. Vertically grown graphene nanostructures (VG-GNs)

In addition to the horizontal growth of graphene sheets and nanostructures on substrates, there has been much interest and development in the vertical growth of graphene nanostructures. For instance, vertical graphene nanowalls, also known as carbon nanowalls (CNWs) or vertically oriented graphene, are multilayer graphene structures oriented in such a way that the graphene honeycomb lattice is perpendicular to the growth substrate, forming wall-like structures. These *vertically grown graphene nanostructures* (VG-GNs) generally consist of varying shapes besides the wall-like or sheet-like nanostructures, including graphene nanostripes (GNSPs) with large length-to-height aspect ratios [61] as exemplified in Figure 3.1(a), and graphene nano-flowers [10, 61] that exhibit extensive branching behavior of quasi-one-dimensional graphene nanostructures. VG-GNs typically grow uniformly over a substrate in random directions, forming a mesh-like graphene mat, as exemplified in Figure 3.1(b) for GNSPs. VG-GNs can grow up to tens of microns in height with interlayer spacings ranging 0.34 ~ 0.37 nm [10], and can have either perfect AB stacking [71] or turbostratic stacking [61]. Additionally, PECVD synthesis of VG-GNs has been accomplished on a variety of substrates such as Cu [61], Ni [72], Al [73], Si [74], graphite [75] and polymers [76]. Although VG-GNs can also be synthesized via thermal CVD [77], in-liquid plasma [78] and electrophoretic deposition [79], PECVD has been the most common method.

VG-GNs are an appealing material for four primary reasons. First, as graphene-based nanostructures, VG-GNs retain various favorable properties of graphene, such as the high electron mobility [61]. Second, the mesh-like network of VG-GNs creates a porous three dimensional architecture of graphene nano-sheets, yielding extremely high surface areas [80]. Third, VG-GN films have abundant exposed edges, which facilitate active electrochemical properties [81] and interesting chemistries [82, 83]. Finally, VG-GNs represent a potential route for large scale production of chemically pure and high quality graphene materials [61].

The favorable properties of VG-GNs have found ways into a variety of applications. Among them, energy-related applications are most common, primarily in supercapacitors [73, 84–96], but also in batteries [97–107], solar energy conversion [108–115] and fuel cells [116–120]. Field emission [121–126] and molecule detection [127–136] are also notable applications. Other applications include memory devices [79], antibacterial coatings [137], semiconductors [138], catalysis [139], magnetic sensors [140], tissue engineering [141, 142], and heat dissipating [143] and hydrophobic coatings [144]. The extensive study of VG-GNs as an energy material and plethora of other proposed applications suggest that VG-GNs may soon become industrially relevant.

In this section we highlight recent progress made in the PECVD fabrication of VG-GNs, including strides made in controlling VG-GN material characteristics, novel synthetic procedures, VG-GN heteroatomic doping, nanoparticle inclusion, and VG-GN thin film coatings. We will also discuss recent progress in the characterization of VG-GNs. Finally, future prospects to advance the field of VG-GNs will be discussed. For reviews describing preliminary aspects of VG-GNs, such as the growth mechanism and the basic synthesis procedures, the readers may refer to References [10, 145]. Additionally, a review describing the use of VG-GNs as field emitters can be found in Reference [146].

3.1. Fabrication progress

Typical PECVD growth of VG-GNs takes place in medium vacuum (10 mTorr ~ 10 Torr), requires a carbon source (*e.g.*, methane), an etchant (*e.g.*, hydrogen) and a radiation source (*e.g.*, microwave) to induce the plasma. Most VG-GNs growth also requires high substrate temperatures (*e.g.*, 800 ~ 1300 K). The radiation induced plasma consists of carbon, etchant radicals and ions. The seeding of VG-GN growth may take place at graphitic defects that form during early growth [10] or directly at the plasma-induced radical sites of the substrate [61]. After a VG-GN is seeded, carbon radicals may continue to deposit and contribute to the growth of VG-GNs, while etchants remove defects and amorphous carbon. More in-depth discussion of typical growth procedures and mechanisms and be found in the review by Bo *et al* [10].

3.1.1 VG-GN material characteristics.

Although VG-GNs are graphene-based nanomaterials, even the highest quality VG-GNs do not demonstrate the ideal properties of two-dimensional graphene [61]. Therefore, research efforts that correlate the growth parameters with the quality of VG-GNs are important to advance this field. Additionally, modifications (*e.g.*, defect incorporation, chemical doping, *etc.*) to VG-GNs can result in certain desirable properties through functionalization at the expense of other properties (*e.g.*, electron mobility). Significant studies in these respects will be discussed in this section.

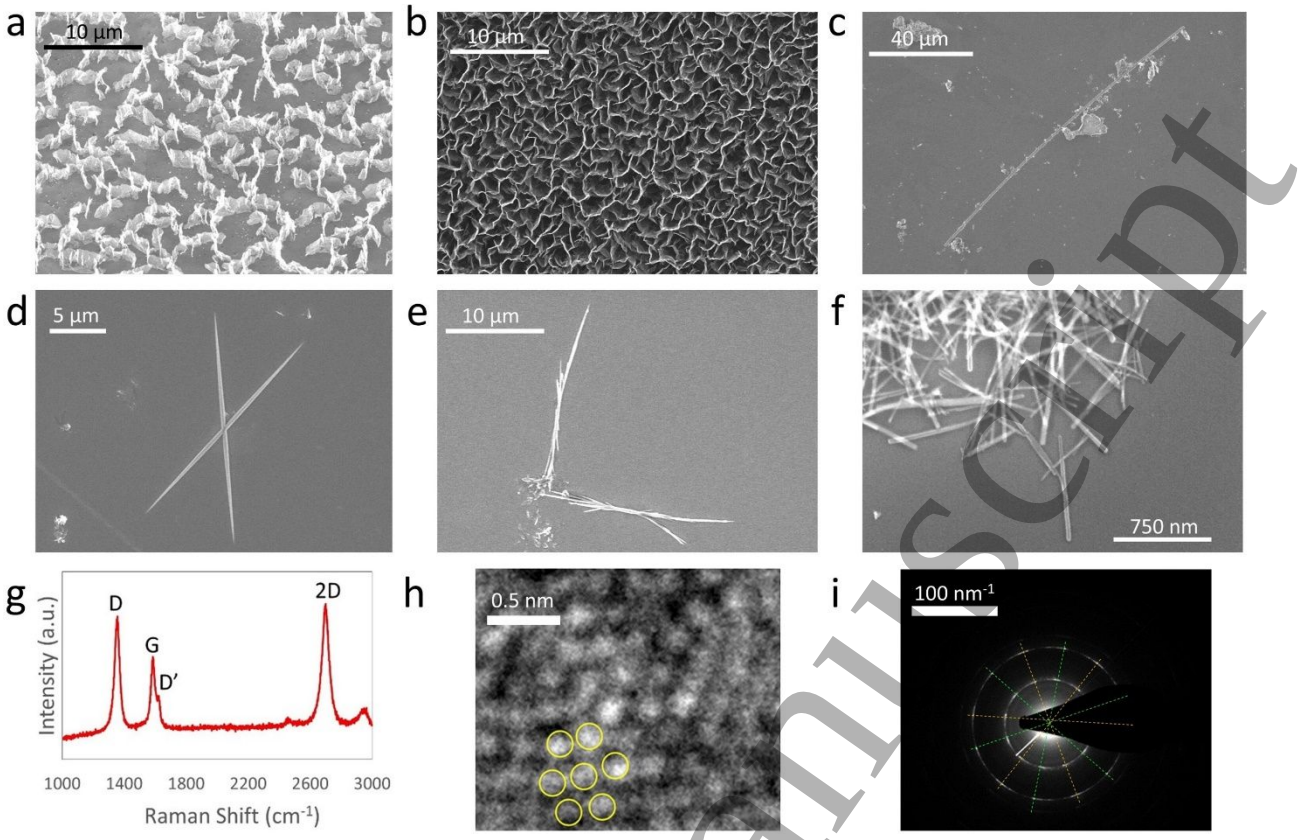

Figure 3.1: Characterization of DCB-catalysed PECVD-grown GNSPs [61]: (a) Tilted (45°) SEM image of GNSPs. (b) Top-down SEM image of as-grown GNSPs. (c) – (f) SEM images of exfoliated GNSPs, demonstrating the variety of graphene nanostructures that can be obtained by exfoliating as-grown GNSPs. The exfoliated nanostructures shown here range in dimensions from 1 µm × 125 µm (panel c) to 30 nm × 1100 nm (panel f). In addition to completely separated individual GNSPs and some interconnected, web-like graphene pieces (panel c), exfoliation also produced two (panel d) or more (panels e and f) GNSPs fused together. (g) A representative Raman spectrum of GNSPs, showing characteristic *D*-, *G*-, *D′*- and 2*D*- peaks. (h) A high resolution TEM image of GNSPs demonstrating the atomic structure. (i) A representative SAED pattern of GNSPs, which reveals two sets of incommensurate six-point patterns (highlighted by the colored lines) overlapping each other, suggesting that this sample consists of multiple graphene layers that are rotated with respect to each other.

Recently, we have demonstrated VG-GN materials with large aspect ratios (>~ 100) by using aromatic molecules in the PECVD growth as the seeding molecules [61]. These VG-GNs are dubbed as *graphene nanostripes* (GNSPs) to emphasize their large aspect ratios and also to differentiate them from *graphene nanoribbons* (GNRs) that typically referred to quasi-one-dimensional graphene nanostructures that exhibit quantum confinement effects [61]. As exemplified in Figure 3.1(c) for an GNSP that was transferred and isolated on a silicon substrate, the GNSP exhibited dimensions of <~ 1 µm in width and 125 µm in length, which corresponded to a large aspect ratio of ~ 125:1.

These GNSPs with large aspect ratios are also high quality materials that can be produced with high yield and at room temperature. We further found that although the as-grown GNSPs formed highly interconnected networks and the distance between joint points was typically short (*e.g.*, 1 µm, see Figure 3.1(b)), long GNSPs could be isolated from samples because GNSPs network joint points did not represent the end of a GNSP, but rather represented splitting points where the multiple GNSP layers split in different directions [61]. This notion was confirmed by studying the SEM images of all transferred samples after sonication in solvent, which always revealed combinations of long and straight GNSPs together with interconnected webs of short graphene pieces, as exemplified in Figure 3.1(c). Moreover, the synthesis involved substituted benzene carbon sources that led to C_6 radicals and C_6H_6, as shown by the representative RGA data in Figure 3.2(b). The presence of C_6 radicals and C_6H_6 molecules in addition to methane played

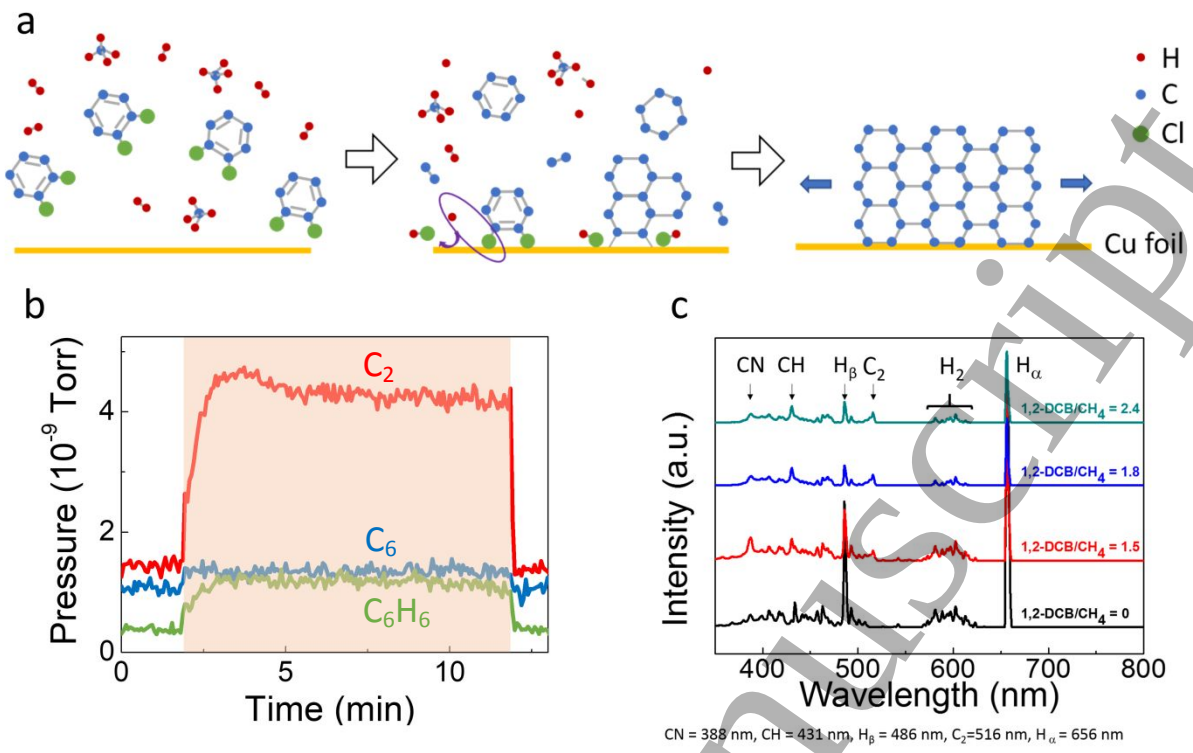

Figure 3.2: PECVD growth mechanism of GNSPs catalysed by DCB [61]: (a) Schematic illustration of a proposed model for DCB-catalysed growth of GNSPs on copper. (b) RGA data of different molecules as a function of time, where the shaded area represents the time interval when plasma is turned on. (c) OES data during the growth of GNSPs for different ratios of DCB to methane.

an important role in the rapid room-temperature growth and the development of GNSPs with large aspect ratios, which was in contrast to typical PECVD growth of VG-GNs that primarily involved C_2 radicals from such carbon sources as hydrocarbon (C_2H_2 or CH_4) and fluorocarbon (CF_4, CHF_3 or C_2F_6). In the latter case the resulting nanostructures were mostly "wall-like" with typical length-to-width aspect ratios <~ 10, whereas the growth rate may be increased with increasing plasma power [10]. Additionally, we found that DCB precursors further enhanced the presence of C_2 radicals (Figure 3.2(c)), which also contributed to the high-yield growth of GNSPs [61].

Hydrophobicity/hydrophilicity is generally an important characteristic of nanomaterials. In the case of graphene, while it is intrinsically hydrophilic, airborne contaminants readily render graphene hydrophobic [147, 148]. Given that many electrochemical applications require hydrophilic electrode materials to be compatible with aqueous solvents and the strong interest in using VG-GNs as electrode materials, several investigations have focused on achieving hydrophilic VG-GNs for various electrochemical applications. In these studies, hydrophilicity (also known as wettability) is quantitively determined by placing a water droplet on a VG-GN surface and then measuring its contact angle with the surface; a decreased contact angle signifies increased hydrophilicity. In the following we discuss two recent studies regarding hydrophilicity of VG-GNs.

Zhang *et al* [74] performed post fabrication argon sputtering of VG-GNs to increase the surface defect content as determined by Raman and x-ray photoelectron spectroscopies. These argon-sputtered VG-GNs with higher defect concentrations were found to be more hydrophilic than as grown VG-GNs, suggesting that the hydrophilicity of VG-GNs can be manipulated via defect engineering.

Subsequently, Shaui *et al* [72] studied the dependence of VG-GN hydrophilicity on the VG-GN areal density. Here the VG-GN areal density is determined by the average distance between individual vertical graphene structures. Shaui *et al* produced VG-GNs with interstructure distances ranging from 15 nm to 306 nm on metallic substrates and demonstrated that hydrophilicity increased with increasing VG-GN areal density. They further showed that the Raman spectra of all samples were nearly identical, suggesting that the defect contents were similar in all samples so that the increased hydrophilicity may be primarily attributed to the increasing VG-GN areal density. Shaui *et al* also conducted supercapacitor measurements and showed that supercapacitor properties in terms of the specific capacitance and specific

energy improved with increasing VG-GN areal density. On the other hand, it was not clear whether the improved properties were due to increased hydrophilicity or increased edge content or both, as the graphene edge states generally have a higher capacitance than the graphene basal plane [81].

In addition to providing the necessary radicals for VG-GNs growth, plasma in the PECVD synthesis contains high energy electrons and ions [149] that can contribute to defects in VG-GNs. The kinetic energy of such charged species is greatest near the plasma source. Cuxart *et al* [75] demonstrated a remote growth of VG-GNs where the growth substrate was not placed directly in the plasma generating medium. Although the VG-GNs thus synthesized were compromised in quality as determined by their Raman spectroscopic characteristics, the demonstration of remote plasma growth was significant because it suggested the feasibility of PECVD growth of VG-GNs on delicate substrates that may be susceptible to high-energy ion bombardment and/or UV-induced damages.

3.1.2 Precursors for the PECVD synthesis.

An important consideration in optimizing the PECVD synthesis of VG-GNs is to achieve reproducible mass production at both reduced costs and minimum environmental impact. A feasible approach is to explore alternative carbon precursors and/or innovative substrates, which may be better suited for particular applications. We review below recent progress in the exploration of different carbon precursors and substrates.

As mentioned previously, we have recently achieved a high yield and single-step deposition of high quality GNSPs by including substituted benzenes in the PECVD growth [61]. Specifically, trace amounts of 1,2-dichlorobenzene were included in a hydrogen/methane plasma, and, despite its low content, the 1,2-dichlorobenzene had significant effects on the growth. Additionally, other substituted aromatics such as 1,2-dibromobenzene, 1,8-dibromonapthalene and toluene were used as precursor molecules for the growth of GNSPs, although 1,2-dichlorobenzene was found to be the most effective [61]. Similarly, Lehmann *et al* [150] reported using paraxylene (a substituted aromatic) in the synthesis VG-GNs, although in their work paraxylene was the sole carbon source and the synthesis was carried under argon gas flow.

A favorable choice of precursors should not only take into consideration of the waste items and natural products but also the cost and accessibility. In this context, evaporated essential oil had been used as a carbon precursor and combined with a hydrogen/argon plasma to produce VG-GNs [151]. Similarly, butter [152], lard oil [153] and sugarcane [154] had been placed on metal substrates and exposed to hydrogen/argon plasmas to produce VG-GNs. Finally, Zhou *et al*. [155] used graphene oxide as a precursor to synthesize VG-GNs by first converting the graphene oxide into a graphene aerogel, then exposing the graphene aerogel to a methane/hydrogen plasma at 1050 K. Although this approach involved several steps and produced VG-GNs with excess oxygen impurities, its novelty is noteworthy.

In addition to novel precursors, different growth substrates have also been demonstrated in recent years. Most notably, VG-GNs had been grown on silicon nanowire meshes with nanowire diameters as small as 37 nm [156]. The resulting composite of VG-GNs on silicon nano-mesh had extremely high surface areas. Besides silicon nanowires, synthesis of VG-GNs on a polymer [76] and aluminum foils [73] has also been demonstrated recently. These results suggest the versatility of PECVD growth so that a variety of precursors and substrates can be tailored with proper growth conditions to specific applications.

3.1.3 Heteroatom doping.

Despite many desirable properties (*e.g.*, high electron mobility), the absence of a bandgap and the relative inert chemical properties of graphene limit its applications to photovoltaics and catalysts, including in fuel cells and electrochemical energy storage. Heteroatom doping, *i.e.*, substitution of non-carbon atoms into the graphene lattice, has been employed to overcome this limitation, and the selection and combination of specific heteroatom dopants determines the performance of the resulting material in applications [157]. Among the heteroatoms that have been incorporated into horizontally grown graphene sheets include boron, nitrogen, sulfur, iodine, bromine, phosphorus, selenium, chlorine, and fluorine [158]. In contrast, fewer heteroatoms have been attempted for doping into VG-GNs, which include nitrogen [93,126,159], boron [121,160,161], and fluorine [162–164]. Interestingly, co-doping of any two heteroatoms to VG-GNs has not been reported. In the following we review the successful doping procedures that have been investigated to date for VG-GNs.

Nitrogen doping of VG-GNs has been achieved during the PECVD growth and via post-growth modification. Specifically, Soin *et al* achieved nitrogen doping by applying a N_2 plasma to VG-GNs grown by a typical procedure [159]. Similarly, Wang *et al*. achieved nitrogen doping by adding ammonia gas during their regular PECVD growth procedure [93]. Interestingly, it was found that simply including N_2 gas flow during the PECVD growth did not result in nitrogen doping [159, 165]. Alternatively, Zhao *et al*. applied an ammonia plasma to readily synthesized VG-GNs and were able to achieve nitrogen doping to VG-GNs [126]. However, such a post fabrication plasma treatment tends to result in inhomogeneous nitrogen dopings, with primary nitrogen concentrations accumulated near the surface of VG-GNs.

Boron doping of VG-GNs has only been achieved during the growth process by including B_2H_6 gas during the PECVD synthesis of VG-GNs [121, 160, 161]. Although the achievement of boron doping is notable, B_2H_6 is dangerous and expensive. Therefore, further exploration of other safer

and more practical means of boron doping would be desirable.

To date surface fluorination of VG-GNs has been achieved in several ways, all of which via post fabrication modification. Satulu *et al*. fluorinated VG-GNs via sputtering of polytetrafluoroethylene polymer and also by exposing VG-GNs to $C_2H_2F_4$ or SF_6 plasmas [162]. They also reported superhydrophobicity in the resulting material. Davami *et al*. achieved fluorination by simple exposure of VG-GNs to XeF_2 [163]. On the other hand, Lin *et al*. achieved fluorination of VG-GNs by cycling gallium ion bombardment and XeF_2 exposure [164]. These studies all reported a significant increase in the mechanical stiffness of fluorinated VG-GNs.

3.1.4 Nanoparticle anchoring.

Development of heterostructures of VG-GNs and various nanoparticles has been explored in an effort to exploit the attractive properties of each component. For instance, electrochemically or catalytically active nanoparticles anchored onto VG-GNs could enable higher surface areas and benefit from the conductive VG-GN network. To date, nanoparticle inclusion into VG-GNs has only been achieved by post fabrication, and the methods used include sputtering [166], atomic layer deposition [102], solvothermal synthesis [167, 168], spin coating [169] and electrodeposition [98, 130]. Anchoring lithium titanate [102], hydrogen molybdenum bronze [98] and molybdenum disulfide [156, 157] nanoparticles to VG-GNs have demonstrated enhanced performance of the resulting heterostructures in lithium and sodium ion batteries. On the other hand, tin oxide anchoring to VG-GNs has shown improved formaldehyde detection [130] and photoelectrochemical performance [169]. In addition, silver, aluminum, cobalt, molybdenum, nickel, tantalum, and silicon nanoparticles have been explored for applications to surface-enhanced Raman spectroscopy [166].

3.1.5 Thin film coatings.

Thin film coatings on VG-GNs have also been reported. Davami *et al* [170] investigated the mechanical properties of VG-GNs coated by thin-film Al_2O_3 and demonstrated a three-fold increase in the Young's modulus of VG-GNs with a 5 nm thick Al_2O_3 coating. Park *et al* [171] sputtered carbon, silicon, and silicon carbide onto VG-GNs and found decreased electrical resistivity in each case. Thin film coating on VG-GNs offers the possibility of creating arbitrary thin films that exhibit the high surface area and significant mechanical strength of the VG-GN networks, which may lead to novel functional composite materials and so is worthy of further exploration.

3.2. Characterization

Characterization of VG-GNs typically aims to demonstrate the synthesis of high quality graphene and any properties that may be useful for a specific application. The most definitive characterization tools to demonstrate the growth of VG-GNs is scanning electron microscopy (SEM) along with Raman spectroscopy. SEM characterization is straightforward and only involves identifying the VG-GN morphology. Detailed analysis of a Raman spectrum can provide a variety of information about the quality of the material, the number of graphene layers, stacking order, defect type, and carrier type and concentration [32, 33, 172]. Additionally, as described in Section 2.1, the characteristic peaks (*G*, 2*D*, *D* and *D*′) of the Raman spectrum of graphene are easily identifiable and so are convenient experimental signatures for confirming the presence of graphitic materials. Exemplifying Raman spectra for PECVD-grown monolayer graphene sheet and GNSPs are shown in Figure 2.1(a) and Figure 3.1(g), respectively. Generally the Raman spectra of pristine graphene monolayer do not include the *D*-band, whereas the Raman spectra of GNSPs and of all VG-GNs always include a *D*-band due to many exposed edges in the nanostructures [61,173]. We further note that the ratio of the 2*D*-band to *G*-band, (I_{2D}/I_G), is an important identifier of graphene quality. The value of (I_{2D}/I_G) typically ranges from 0.5 to 2, depending on the number of layers, stacking order, carrier concentrations, *etc.*

Besides SEM and Raman spectroscopy, the next most common characterization methods include transmission electron microscopy (TEM), selected area electron diffraction (SAED), and x-ray photoelectron spectroscopy (XPS). The extreme resolution of TEM allows for imaging the edge structure of VG-GNs so that the number of layers can be revealed [173] and even individual atoms of the graphene lattice can be resolved [61]. SAED, typically performed in the TEM instrument, has been employed to determine the crystallinity of VG-GNs. From the SAED studies, it is found that VG-GNs have shown either pristine graphene stacking [71] or turbostratic (*i.e.*, misaligned) stacking [61], although it is still unclear which growth parameters may influence the stacking order of VG-GNs. Examples of a TEM image and a SAED pattern of GNSPs are shown in Figures 3.1(h) and 3.1(i), respectively. The hexagonal graphene lattices can be seen in the TEM image, and the SAED shows two overlapping six-point patterns, implying that the sample has turbostratic stacking, whereas a single six-point pattern would indicate regular stacking [174].

XPS characterizations can provide critical information for the chemical purity and/or heteroatom doping content of the VG-GNs [93]. Additionally, high resolution spectra of the carbon 1s peak can indicate the relative content of sp^2 and sp^3 hybridized carbon, which is an indicator of the defect concentration and the quality of VG-GNs [74]. Ganeson *et al* [175] performed a detailed comparison of XPS and Raman

spectroscopy measurements of VG-GNs and suggested that the two techniques in tandem could provide information about the type of defects present.

Other useful characterization methods include ultraviolet photoelectron spectroscopy (UPS) for measuring the work function of VG-GNs [176, 177], which provides useful information about the doping level of the graphene nanostructures; wettability studies, where the contact angle of a water droplet on the VG-GN sample is determined [72, 74]; surface area measurements via nitrogen adsorption Brunauer-Emmett-Teller (BET) method [178]; and electrical transport measurements that determine the resistivity, carrier concentration and electron mobility [61, 179, 180]. In addition, certain application-specific characterizations, such as the cyclic voltammetry measurements, are carried out to evaluate the performance for energy storage applications.

While the research field of VG-GNs has largely focused on applications and novel fabrication procedures, some notable characterization of the novel properties of VG-GNs have been made in recent years, which we summarize below.

3.2.1 Long term stability measurements.

Ghosh *et al* [181] and Vizireanu *et al* [182] performed stability measurements on VG-GNs but found contradictory results. Ghosh *et al* exposed VG-GNs to ambient conditions for six months and consistently performed Raman spectroscopy, XPS, hydrophillicity and electrical transport measurements. All of these measurements indicated stable materials [181]. On the other hand, Vizireanu *et al* found immediate changes in the hydrophillicity, and demonstrated time-dependent chemical and morphological modifications via Fourier-transform infrared spectroscopy, XPS and atomic force microscopy [182]. Although the origin for these incongruous findings is not clear, it may be the result of differences in the defect/edge/impurity type and concentration afforded by the different synthetic procedures used in each study. Further studies to correlate the growth conditions and the stability of VG-GNs will be beneficial to controlling the quality and optimizing the functionalization of these nanomaterials .

3.2.2 Pressure dependence and thermal conductivity.

Mishra *et al* [183] performed studies of the VG-GN pressure dependence and thermal conductivity. Pressure dependent shifting of the Raman modes revealed a reversible deviation from the long-range structural order under pressures exceeding 16 GPa. Mishra *et al* suggested that their findings in the VG-GNs closely correlated with the pressure dependent properties of seven-layer graphene sheets. They further confirmed via TEM that the thickness of their VG-GN samples was indeed consistent with seven layers of stacked graphene. Hence, the pressure dependence of VG-GNs behaved similarly to that of large area graphene sheets of comparable thicknesses despite the differing geometries. Mishra *et al* also determined the thermal conductivity of VG-GNs via temperature dependent Raman spectroscopy [183].

3.3 Outlook for future development of VG-GNs

The most significant hindrance in the development of VG-GN research stems from the complexity of plasma chemistry, which is sensitive to the gas composition and flow rate, plasma source and plasma power, precursor type, substrate material, growth chamber dimension, *etc.* [149]. Given that different research groups employ varying PECVD deposition systems, it is generally difficult to exactly reproduce the experimental conditions in different laboratories. In this context, studies that investigate a single growth parameter (*e.g.*, the flow rate) are not particularly effective in advancing the development of VG-GNs for applications. On the other hand, although exact experimental conditions may be difficult to fully reproduce, VG-GNs of comparable characteristics can still be developed in different systems. Thus, the development of VG-GNs can benefit substantially from high-standard and more thorough characterizations, especially in application-focused studies.

In particular, more detailed Raman spectroscopic and XPS studies could provide much better insights into the microscopic properties of VG-GNs. For instance, most studies simply use Raman spectroscopy to confirm the presence of graphene by citing the characteristic *D*, *G* and 2*D* bands. On the other hand, simple peak fitting would provider much more information, such as the *G* peak position and the 2*D* peak symmetry that offer information about the stacking order of graphene layers [48,61,172]; the intensity ratio of the *D* to *G* peaks indicates the crystallite size [61,172] according to the relation in Equation (2); the *G* and 2*D* peak positions indicate doping content [172]; and the intensity ratio of the *D* to *D*′ peaks can indicate the type of defects present, *i.e.*, edge, vacancy, graphitization, *etc.* [175]. XPS can reveal the relative content of sp^2 and sp^3 hybridized carbon bonds, carbon vacancy defects, functionalization and even the structural quality [175]. These exemplary studies demonstrated by Ganesan *et al* [175] are highly informative and can be standardized for meaningful comparison of the physical properties of VG-GNs produced by different groups under varying growth conditions.

In addition to standardizing the characterization of VG-GNs, better methodology in the following prospects would significantly advance the research of VG-GNs.

3.3.1 Defect characterizations.

Although Ganesan *et al* [175] have demonstrated XPS and Raman spectroscopy characterization of VG-GNs whereby the type and concentration of VG-GN defects was quantified, more rigorous validation of this characterization method is still needed. Specifically, the conclusions deduced by Ganesan *et al* [175] depended on results associated with

monolayer graphene, whereas VG-GNs are generally multilayer structures. In order to validate the findings of Ganesan *et al*, further studies that correlate XPS and Raman spectroscopy measurements with direct microscopic observation of the defects (*e.g.*, STM and TEM imaging) would be particularly informative. Such correlation could expedite the optimization of growth parameters for VG-GNs to achieve desirable properties towards specific applications.

3.3.2 Computational modelling.

In addition to more rigorous and standardized characterization of VG-GNs, computation modelling for the complex PECVD growth process can significantly advance the field. For instance, although a phenomenological model was proposed for the catalytic single-step growth process of GNSPs [61], this model only considered the role of the carbon source and the etchant in a very basic manner. On the contrary, even a simple hydrogen/methane plasma involves dozens of chemical species and radicals of different kinetic energies [149], so that the complicated interplay of all chemical species in the growth process of VG-GNs cannot be well understood without computational modelling. Better understanding of the influence of all plasma species on the VG-GN growth process via computational modelling can also help guide the synthesis procedure to achieve desirable properties of VG-GNs.

3.3.3 Solution processing and transfer of VG-GNs.

Although VG-GNs can be grown on a variety of substrates so that pertinent substrates may be chosen for specific applications, not all materials can withstand the PECVD environment that involve energetic ions, electrons, radicals, UV emission and at times relatively high temperatures. Solution processing, *i.e.*, suspension of VG-GNs in solution and removal of them from substrates compatible with the PECVD process so that they can be transferred to other substrates, would expand the potential applications of VG-GNs. Furthermore, solution processing can enable additional characterizations of VG-GNs by dispersing them, including analysis of the aspect ratio and conductivity of individual graphene nanostructures.

3.3.4 Heteroatom doping

As discussed previously, heteroatom doping can expand the properties of graphene by functionalization. However, heteroatom doping has not been well explored in VG-GNs. Further, the doping of VG-GNs that has been explored to date often involves dangerous and expensive gases. Expanding the palette of heteroatoms and establishing safe and cost effective dopings of VG-GNs would enable further application of VG-GNs.

VG-GNs research is a fast-growing field due to the myriad of their potential applications. In particular, VG-GNs can offer many of the attractive properties of graphene and graphene-based, functionalized nanomaterials with the possibility of scalable syntheses. Certain properties of VG-GNs, such as the defect content and hydrophillicity, can also be controlled. Additionally, nanoparticle inclusion and heteroatom doping provide an even broader range of possibilities. In recent years, major progress has been made in the fabrication and modification of VG-GNs to tailor their properties for specific applications. Advances in better characterizations of VG-GNs have also been developed. By holding a high standard of characterizations as well as pursuing computational modelling and developing proper transfer methods, we expect further progress in the understanding and control of the VG-GN growth mechanism, which can further enhance current applications and enable new applications of VG-GNs.

4. Carbon nanotubes (CNTs)

Among all vertically grown graphene-based nanomaterials, CNTs are one of the most promising substances that have been widely used in many fields. Made of rolled-up single or multiple graphene sheets, CNTs retain most of the excellent properties of graphene while exhibit additional quantum behaviour due to its one-dimensional structure. In the case of single-wall carbon nanotubes (SWCNTs), they can be either semiconducting or metallic, depending on the chiral vector of the nanotube in real space [184]. SWCNTs exhibit semiconducting property with bandgap around 0-2 eV when they have zigzag structure. Armchair SWCNTs are metallic with band degeneracy between the highest π valance band and the lowest π conduction band at the K-point. The three-dimensional (3D) structures of different helicities are illustrated in Figure 4.1. On the other hand, multi-wall carbon nanotubes (MWCNTs) are typically metallic [184]. The electrical conductivity of CNTs can be up to ~ 10^5 S/cm [185], which implies high charge transport capability. CNTs can be synthesized either aligned or unaligned. Although CNTs with random distribution are often sufficient for most applications, aligned CNTs are highly desirable for vertically stacked, layer by layer device structures.

The typical diameters of SWCNTs are around 0.8-2 nm, whereas those of MWCNTs can be as large as hundreds of nanometers. The lengths of CNTs range from tens of nanometers to centimeters. The usual aspect ratio (length/diameter) is in the range 10^2–10^4 [186, 187]. Apart from high electrical conductivity, CNTs also exhibits a high thermal conductivity (~ 6000 W/m•K), which is five times higher than copper. Moreover, CNTs exhibit high thermal stability up to 2800 °C in vacuum. The mechanical property of CNTs can be up to 45 billion Pascal (tensile strength), which is 100 times stronger than stainless steel [188]. These interesting properties make CNTs very attractive material for many applications, including in organic solar cells [189-191],

fuel cells [192, 193], batteries [194], supercapacitors [195, 196], water filters [197], and biosensors [198, 199].

4.1. Common synthesis techniques

CNTs are commonly synthesized by three techniques: the arc-discharge method, laser-vaporization technique, and chemical vapour deposition (CVD). The initial discovery of CNTs involved the arc-discharge method, in which carbon vapour was formed by an arc discharge between two carbon electrodes under inert atmosphere [200]. A direct current generated a very high temperature discharge (~ 2000–3000 °C) between the two electrodes and both SWCNTs and MWCNTs could be synthesized. To date this method remains the most common and easiest to grow CNTs. On the other hand, the purity of resulting CNTs is generally poor because metallic particles and amorphous carbons can always be found along with CNTs, even though the CNTs products from this method are usually well-crystallized,

In contrast, the laser-vaporization technique can easily produce high-purity CNTs. The mechanism for the formation of CNTs by laser-vaporization is similar to the arc discharge method. Specifically, a high-purity graphite chunk is placed into a high-temperature furnace with catalytic metals such as Ni, Co, Pt. The graphite chunk is targeted and ablated by a high-power laser; CNTs are thus formed and brought to a copper collector [201]. Although laser-generated CNTs are usually of high purity, their growth yield is usually very low, making this technique inefficient for industrial applications.

In comparison with the aforementioned CNT synthesis methods of arc discharge and laser vaporization, CVD has been found to be a much better solution and is still the most popular method these days. In particular, CVD synthesis of CNTs is a practical and scalable technique suitable for mass production. Recently, PECVD synthesis of CNTs has been developed and is found to be even better than the thermal CVD (T-CVD) method. In this section, we review methods of CNT synthesis by T-CVD and PECVD, and also discuss the latest progresses in this field.

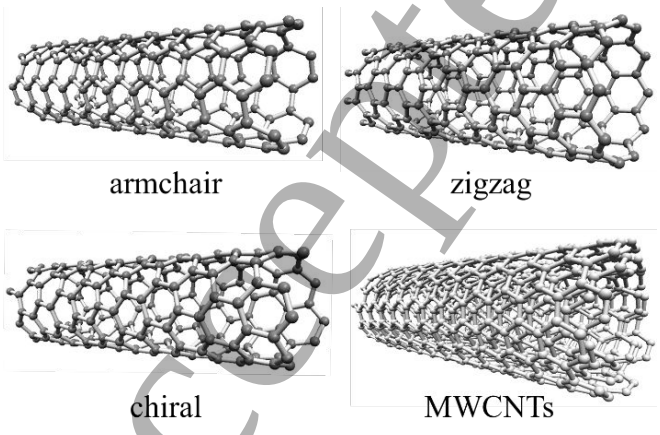

Figure 4.1 Schematic illustrations of 3D structures of SWCNTs with different helicities and MWCNTs.

4.1.1 Thermal CVD synthesis of CNTs

A simple schematic diagram of a T-CVD setup is shown in Figure 4.2. A typical T-CVD process involves a catalyst-coated substrate, which is placed inside a quartz tube. The entire growth system is evacuated down to around 10-300 Torr by a mechanical pump. The precursor gases are then introduced through the tubular reactor while the tube is heated up to a desired temperature, typically 600-1200 °C. The flow rate of hydrocarbon gases as well as the temperature should be accurately controlled so the precursors can be decomposed to provide reactive hydrocarbon for CNTs formation. The presence of activated carbon molecules or clusters in gaseous phase is critical for the growth process. Commonly used gaseous carbon precursors include acetylene, methane, ethylene, xylene and carbon monoxide. These carbon sources can be gaseous, liquid, or even in solid state form. In the case of liquid precursors, the liquid is placed in a flask and usually an inert gas is pressured through it to push the hydrocarbon vapour to the reaction zone. Elevated temperatures can also be applied to increase the evaporation rate of liquid precursors. In the case of solid precursors, they may be directly kept in the upstream zone of the reaction furnace. Some volatile solid materials such as camphor and ferrocene can directly turn from solid to vapour and then be introduced into the reactor as carbon sources. After these hydrocarbons have been introduced into the system, CNTs can then start to grow on the catalyst-coated substrate in the tubular reactor. After the growth process is completed, the furnace is slowly cooled down to room temperature and CNTs are collected from the substrates. Details of the catalysts and precursors will be further discussed in the following subsection.

4.1.2 PECVD synthesis of CNTs

In the case of PECVD synthesis of CNTs, the growth conditions and mechanism are very different from those of

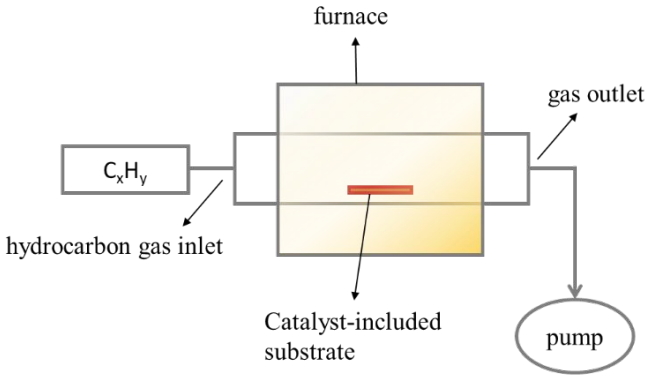

Figure 4.2 Schematic diagram of a thermal CVD setup for CNTs synthesis.

using thermal CVD reactors. While thermal CVD uses heat to provide the necessary energy to decompose hydrocarbon and to create reactive dangling bonds, PECVD processing generates electromagnetic fields to ionize hydrocarbon molecules and create radicals. A typical environment for PECVD synthesis of CNTs is schematically shown in Figure 4.3. A catalyst-included substrate is placed on a sample holder in the growth chamber. The catalyst-included substrate can be a pure metal, such as copper or nickel, or metal-coated materials. Various hydrocarbon gases of different partial pressures are introduced into the growth tube before the plasma is turned on. Additionally, carbon-based precursors are widely used to promote CNTs formation by providing extra carbon sources. Some of the commonly used precursors as well as several novel precursors will be further discussed in the following subsections. The plasma cavity is placed in a position that covers the entire substrate surface area. After lighting up the plasma, the resulting strong electromagnetic field begins to ionize the hydrocarbon gases inside the growth chamber and create reactive radicals around the substrate. At the same time, the plasma can also heat up the catalyst surface and provide more energy for reactions. Certain large radicals or ions can even be accelerated by the electromagnetic field and then bombard the substrate surface to create nucleation sites for the growth of CNTs. When hydrocarbon radicals reach the reactive substrate surface, they start to form bonds and become the bases of CNTs. If correct conditions are chosen, stable plasma will continue to generate carbon sources so that deposition of CNTs occurs on the substrate. The presence of homogeneous plasma in a large region can deposit CNTs over a large area, up to centimeters in scale. Generally speaking, the catalyst-included substrate for CNTs deposition is located in the region where plasma is applied, and the growth of CNTs usually takes place following the direction of the plasma field. At the same time, the vacuum pump of the PECVD system removes the excess hydrocarbon molecules and radicals, thereby preventing the formation of clusters of amorphous carbon.

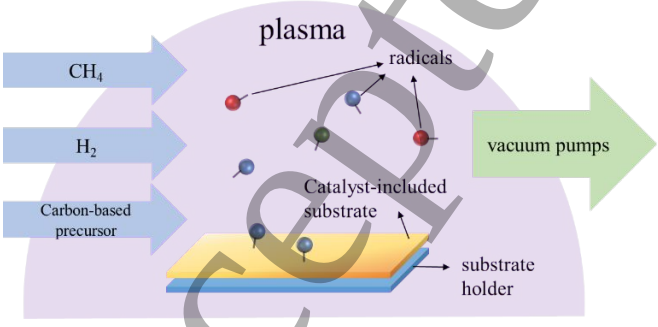

Figure 4.3 Schematic illustration of a PECVD growth environment (with carbon sources, precursors, hydrogen plasma and various radicals) for CNTs synthesis on a catalysed substrate.

As discussed in Section 1, typical plasma sources include direct-current (DC) discharge plasma, radio frequency (RF) plasma, and microwave (MW) plasma, which provide various energy densities in a local volume. Among them, MW plasma is the most common choice for CNTs synthesis. As compared to the thermal CVD, the use of PECVD makes it possible to achieve deposits with higher yields of CNTs at a relatively low temperature because the gas molecules can be decomposed more efficiently by the strong electromagnetic field.

4.2. Precursors and catalysts

The precursors and catalysts are the two primary factors that induce the CNTs growth in both thermal CVD and PECVD systems. We discuss some of the important precursors and catalysts in the following subsections.

4.2.1 CNTs precursors

As mentioned before, carbon containing compounds have been widely used as precursors to grow different kinds of CNTs. The most commonly used precursors are methane [202], ethanol [203], carbon monoxide [204], ethylene [205], acetylene [206], benzene [207], and toluene [208]. These precursors, especially acetylene and methane, are used to synthesize CNTs in some early reports with various kinds of catalysts [209]. In 2002, Maruyama *et al.* demonstrated the use of alcohol as the carbon source to deposit high-purity SWCNTs in a relatively low-temperature CVD system [210]. Owing to the etching effect of OH radicals attacking carbon atoms with their dangling bonds, Maruyama *et al.* found that side products such as amorphous carbon, multi-walled carbon nanotubes, metal particles and carbon nanoparticles are all significantly suppressed even at a relatively low reaction temperature < 800 °C. Since then, alcohol has become a popular precursor to grow low-cost, large-scale, and high-purity SWCNTs in CVD systems. In 2004, Hata *et al.* introduced an efficient CVD synthesis method for SWCNTs where the activity and lifetime of the catalysts were enhanced by water [211]. The catalytic activity enhanced by water results in massive growth of very dense and vertically aligned nanotube forests with heights up to 2.5 millimeters. Moreover, the CNT product can be easily separated from the catalyst-included substrate, providing nanotube material with purity above 99.98%. There have also been a few kinds of new precursor explored. For example, in 2011, Zhao's group used sesame seeds as a precursor to grow CNTs [212]. By using this natural organic precursor consisting of uniform microcells with a Fe-complex, the authors found that the Fe-complex could release uniformly-distributed Fe nanoparticles, which efficiently produced CNTs arrays with lengths up to 100 μm. The aforementioned results suggest that carbon-included precursors play crucial

roles in the growth of CNTs. Thus, by proper selection of the precursors as well as fine tuning their flow rates during the growth, the quality and yield of CNTs can be significantly improved.

4.2.3 CNTs catalysts

Apart from the precursors, catalysts are also critical for CNTs growth by providing a more reactive environment for hydrocarbon decomposition in a relatively low temperature environment. Metallic nanoparticles are the most common materials used for catalysis. In particular, Fe, Co and Ni nanoparticles are the most favoured catalysts for CNT syntheses because of their high solubility for carbon, high carbon diffusion rates, and high adhesions with CNTs when compared with other transition metals [213]. Recent studies have further indicated that other metals such as Cu, Au, Mg, Al and Sn can also be used to catalyse the synthesis of CNTs [214-216]. Although these metals have lower solubility for carbon in their bulk form, the solubility of the corresponding nanoparticles actually increases substantially when the diameter of the nanoparticles is smaller than 5 nm. In addition to metallic nanoparticles on substrates as catalysts, substrates coated by metallic thin films as catalysts have been shown to successfully grow CNTs [217]. Moreover, alloys have been found to exhibit higher catalytic activities than simple metallic elements. More recently, Ni–Mo and Co–Mo alloy nanoparticles were used for catalytic CVD synthesis of CNTs [218]. These findings showed that the synergism between two metals in an alloy resulted in large-scale production of non-bundled, few-walled CNTs with a small spread of diameter distributions and of high quality. On the other hand, studies have revealed that metals are not necessary for catalysing the growth of CNTs [219]. Additionally, oxygen was found to play an important role in activating the growth of CNTs [220]. Noting that metals are simply catalysts that assist CNT synthesis, we believe that CNTs can grow without the presence of any metal as long as the precursor is sufficiently reactive to decompose the hydrocarbon source efficiently.

4.3. Growth mechanisms

Since the discovery of CNTs, there have been numerous models proposed for the growth mechanisms. Although no specific model can account for all findings from different growth conditions, a few basic notions for the CNT growth process via metallic catalyst have been commonly accepted and are briefly described below. Firstly, upon contact with reactive metallic particles, hydrocarbon vapour decomposes into carbon and hydrogen ($C_nH_m \rightarrow nC + ½\ mH_2$), where the metallic nanoparticles can be heated up and become reactive nucleation sites by arcs, laser, furnace, or plasma sources. Secondly, the decomposed hydrogen gas is pumped away while the remaining carbon starts to dissolve into the metallic catalyst until reaching its solubility limit. Finally, continuous carbon deposition on the metallic nucleation sites leads to the growth of CNTs through two different processes: root-growth and tip-growth.

As shown in Figure 4.4(a), when the metal-substrate adhesion is strong, initial hydrocarbon decomposition and carbon diffusion occurs on the metal surface while the catalyst stays at the bottom. Thus, a hemispherical cap of carbon forms on the metal nanoparticle surface first, and subsequent hydrocarbon decomposition takes place at the circumference on the lower part of the cap, forming a new layer and pushing the cap upward. Given that CNTs grow with the catalyst particles rooted on theirs bases, this growth process is known as the "root-growth model". As long as the catalyst nanoparticles remain reactive and hydrocarbon radicals can reach the root of the CNTs, nanotubes will continue growing longer and longer. On the other hand, when the metal-substrate adhesion is weak, as shown in Figure 4.4(b), hydrocarbon decomposes on the metallic catalyst surface first, and then the carbon atoms diffuse down through the reactive metal, pushing the metallic nanoparticles off the substrate. This growth process is known as the tip-growth model. As long as the metallic top is still open for fresh hydrocarbon decomposition, carbon atoms will continue to deposit and diffuse downward to make the CNTs longer.

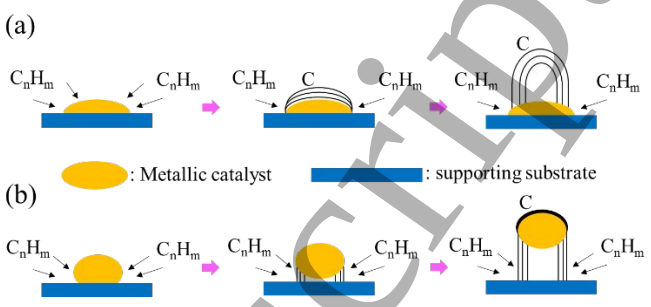

Figure 4.4 Commonly-accepted growth mechanisms of CNTs on metallic catalysts: (a) root-growth model, (b) tip-growth model.

The aforementioned mechanism is a typical model for the growth of vertical aligned CNTs (VACNTs). While in VACNTs the uniform alignment for carriers transport are generally beneficial to the development of vertically stacked electronics such as photovoltaics and OLEDs, horizontally aligned CNTs (HACNTs) are also industrially very important because of their potential applications to transparent displays, astronics materials, field emission transistors, and aeronautic devices due to their extraordinary mechanical, thermal and electrical properties. HACNTs usually follow the free-growth model and so exhibit weak inter-tube interactions,

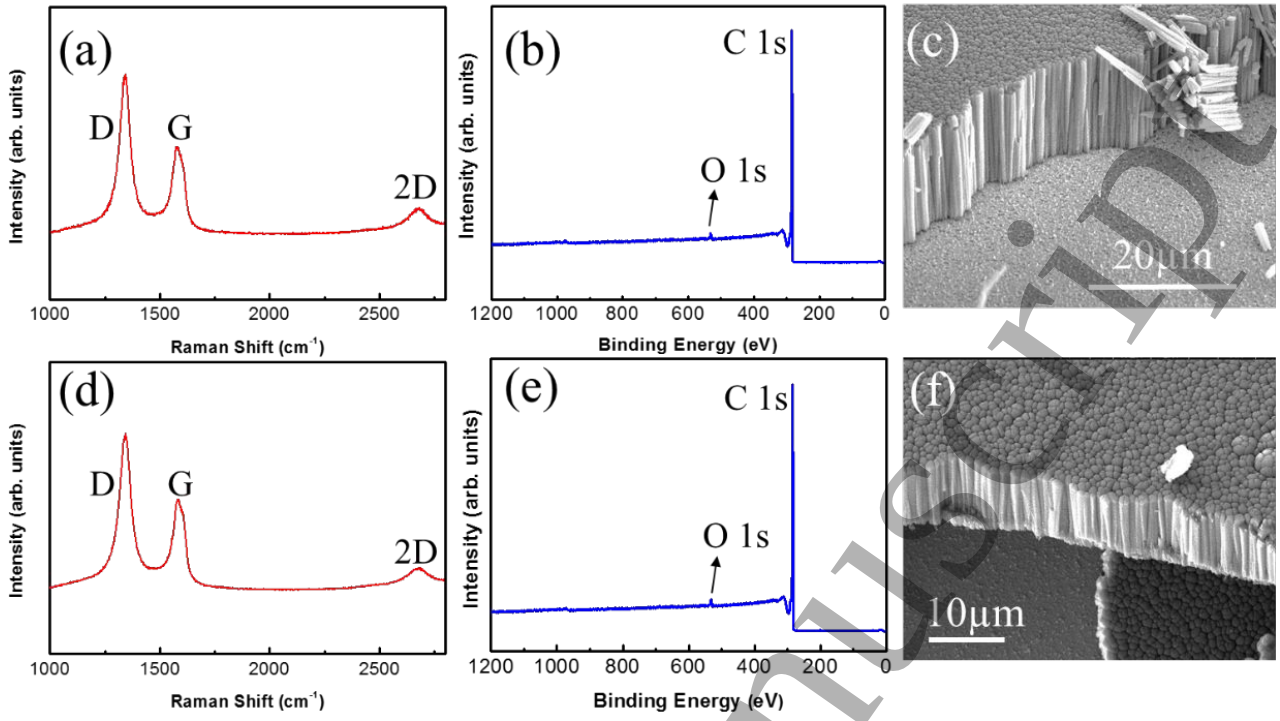

Figure 4.5 Characteristics of DCB catalysed PECVD-grown MWCNTs on different substrates: (a) Raman spectrum, (b) XPS and (c) SEM image of MWCNTs grown on copper foil substrate; (d) Raman spectrum, (e) XPS and (f) SEM image of MWCNTs grown directly on silicon substrate.

leading to low defect densities and ultra-long tube lengths. The synthesis environment of HACNTs is similar to that for VACNTs except the gas flow inside the growing chamber is strong enough to guide the CNT growth direction parallel to the substrate. In addition, a temperature difference between the gas flow and the substrate must be created to produce a thermal buoyancy vertical to the sample [221]. The buoyancy in the laminar gas flow will lift the CNTs from the substrate and the catalyst nanoparticles at the tip ends of the floating CNTs can continue to catalyse the CNT growth. The weak CNT-substrate and CNT-CNT interactions are the main reasons to result in the high quality and ultra-long lengths of HACNTs.

4.4. Latest progresses of CNTs

Despite the fact that CNTs have been discovered for more than 20 years and numerous synthesis methods have been well developed, continuing efforts are being made to further improve the growth processes in order to achieve more efficient synthesis of higher quality CNTs. Here we review some of the latest developments of novel synthesis methods within the past three years.

In 2016, Kar *et al.* used microwave PECVD to synthesize CNTs along with nano-crystalline diamond and graphene nano-walls [222]. By changing the argon gas flow rate as well as the growth time, Kar *et al.* were able to achieve synthesis from nano-crystalline diamond to micro-crystalline diamond, and to CNTs on different substrates. The length and density of CNTs could be well tuned through changing the growth time from 60 to 150 min. Also, in 2017, Gentoiu *et al.* used a PECVD system based on low pressure expanding RF plasma jet generated in argon, acetylene, and hydrogen mixture to synthesize three kinds of nanostructures: vertical aligned CNTs, amorphous carbon nanoparticles, and carbon nano-walls [223]. They found that the deposition temperature was a critical parameter for the growth of different kinds of nanostructures. In particular, the vertical aligned CNTs were obtained at a low temperature of 200 °C. In 2017, Liu's group found that applying Ar^+ ion bombardment during the PECVD growth of CNTs can effectively remove redundant carbon layers on the surface of large catalyst particles, resulting in better growth conditions [224].

Recently, we have employed DCB as the precursor to synthesize GNSPs on Cu foil [61]. Noting that DCB is a highly reactive precursor and can help grow vertical nano-

walls or nanostripes, we investigated the feasibility of using DCB as a precursor to grow CNTs on different substrates, including pure Cu foils, a thin layer of Cu (~ 30 nm) on Si substrates, and pure Si substrates. Figure 4.5(a) shows the Raman spectrum of the MWCNTs thus synthesized. Three distinct peaks were found and assigned at 1346 (*D*-band), 1588 (*G*-band), and 2691 (2*D*-band), confirming the formation of CNTs [225]. The prominent *D*-band peak may be attributed to the large amount of domain boundaries near the tip area of the MWCNTs. As shown by the SEM image in Figure 4.5(c), these MWCNTs are very well aligned alone the vertical direction and are relatively consistent in their diameters (~ 300 nm) and lengths (~ 20 μm). Therefore, when laser light of a Raman spectrometer focuses on the carpet-like MWCNTs surface, the signals are primarily dominated by response from the tip part of the MWCNTs.

In the DCB catalysed PECVD growth of MWCNTs, given that all gases including CH_4, H_2, and DCB vapour are introduced at the same time, the growth technique is an efficient single-step process. Moreover, the yield of MWCNT production can reach around 3 mg on ~ 1 cm^2 substrate area within 10 minutes without the need of any active heating of the substrate, indicating that the new growth method is highly promising to achieve an industrial scale mass production. Moreover, noting that the effective substrate temperature in the PECVD growth process without any active heating is relatively low (<~ 400 °C) as compared to those of typically thermal CVD processes, the synthesis process is compatible with existing device processing in semiconductor industries. Given that no additional Cu nanoparticles are needed to nucleate the CNT growth, it is likely that DCB precursors, various radicals and ions in the plasma play the dominant role in producing the nucleation sites on the substrate surface. Further investigation will be necessary to reveal the exact growth mechanism.

In addition to their uniform dimensions and high-yield growth, XPS spectroscopic studies of the CNT "carpet" surface revealed predominantly carbon 1s signal with a very small oxygen 1s signal as shown in Figure 4.5(b), suggesting high-purity of the CNTs. Thus, these pure, well-aligned and uniform CNTs with a high-yield production rate are promising for a range of applications, especially in the case of electronic devices. Moreover, Raman spectroscopy, XPS, and SEM characterizations of the CNTs grown on Si substrates are found to be comparable to those grown on either Cu foils or Cu thin films, as exemplified in Figure 4.5(c) to 4.5(e). These findings suggest that the single-step, DCB-catalysed PECVD growth technique is not only high-yield without the need of active heating, but also template-free and metallic catalyst-free, which seems significantly more advantageous for industrial applications than all other PECVD and T-CVD growth methods to date and is therefore worthy of further exploration.

Recently, oxygen and oxygen containing species were also found to be crucial factors to affect the growth quality and yield of CNTs in addition to the well-known catalyst effect. For instance, Liu *et al.* studied the synthesis of SWCNTs by using both Si and SiO_2 nanoparticles (NPs) as catalysts [226], and found that the use of SiO_2 NPs yielded much better nucleation and growth of SWCNTs. Their DFT calculations suggested that oxygen atoms could enhance the capture of -CH_x and thus improve the growth of SWCNTs on SiO_x NPs. In 2017, Zhang *et al.* also found that adding 1% oxygen to methane in the PECVD growth process could provide highly reproducible growth of densely packed SWCNTs [227]. They further demonstrated that reactive hydrogen species were generally unfavorable to CNTs formation because they could etch away the deposited CNTs. Based on the aforementioned results, Zhang *et al.* proposed that the key role of oxygen was to balance C and H radicals by providing a C-rich and H-deficient condition to favor the formation of sp^2-like graphitic SWCNT structures.

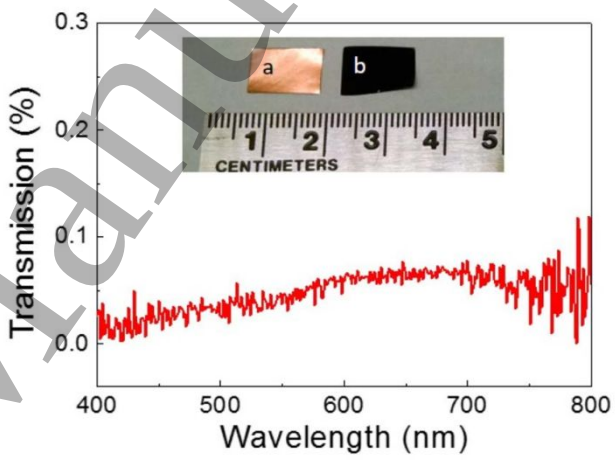

Figure 5.1 Evidences of strong optical absorption by GNSPs: The main panel shows the optical transmission spectrum of GNSPs for wavelengths from 400 nm to 800 nm, revealing transmission < 0.1% for the entire range of wavelengths. The inset shows micrographs of a copper substrate **(a)** before and **(b)** after the growth of GNSPs. The growth parameters for the micrograph in (b) are given in the last row of Table 1. Here we note that the transmission spectrum was obtained by using a Cary 5000 absorption spectrometer with an integrating sphere, and the GNSPs were transferred from the Cu substrate onto a quartz substrate for the optical measurement. The incident light was sent through the entire GNSP sheet and the underlying quartz substrate and then was collected by a detector. The baseline signal of the spectrum was obtained by subtracting the transmission signals from a blank quartz substrate as the reference.

4.5. Current challenges and potential directions for the synthesis of CNTs

Despite substantial progress made over the years, numerous issues associated with the synthesis of CNTs still need to be resolved in order to fully realize their potential for a wide range of applications. We summarize below what we consider as the major challenges and potential new directions for PECVD growth of CNTs.

1) Proper control of the synthesis procedure and the resulting quality of CNTs will require better understanding of the PECVD growth mechanisms under different growth conditions.
2) For the growth of SWCNTs, chirality control is a major challenge. Only when the chirality be well controlled can we obtain desirable SWCNTs.
3) In the case of MWCNTs, controlling the diameter and number of walls is another important issue to address.
4) Catalytic PECVD growth of CNTs appears promising for realizing a low-temperature and high-yield production of high-purity CNTs for industrial applications. More systematic efforts in the development of such techniques are worthy of exploration.
5) Further development of template-free and metal-free methods for synthesizing CNTs will be important to broaden the scope of CNT applications.

5. Discussion

In this section we discuss important issues associated with further development of PECVD and related techniques for graphene growth and applications.

5.1. Effects of geometric dimensions

We have thus far focused largely on how different PECVD growth conditions would result in graphene and graphene-based nanomaterials of varying geometric dimensions. Given that certain physical properties of graphene and graphene-based nanomaterials are strongly dependent on their geometric dimensions, it is highly desirable to develop better understanding of the PECVD growth process and parameters in order to achieve better control of these characteristics. For instance, a pure monolayer graphene sheet is gapless and largely transparent (~ 97% optical transmission) [228, 229]. On the other hand, pure GNSPs are found to exhibit strong optical absorption (with < 0.1% optical transmission) over a wide spectrum [61], as manifested in Figure 5.1. Moreover, we found that exfoliated GNSPs, such as those shown in Figures 3.1 (c)-(f), revealed intense photoluminescence (PL) over a wide spectrum, similar to those found in semiconducting nanowires [230-233]. These broadband optoelectronic properties (up to ~ 4 eV) are clearly beyond simply quantum confinement effects [234] of graphene and are likely the consequence of multiple photon scattering in high-mobility graphene nanostructures, leading to strong coherent interferences and localization of photons that may be exploited for applications to photodetectors, photovoltaic cells, light emitting diodes, and nanolasers. In particular, the high quantum efficiency of pristine graphene [235-237] together with its gapless nature provides unprecedented broadband response in high-purity/mobility GNSPs when compared with traditional semiconducting nanowires. Thus, PECVD synthesis of high-quality GNSPs provides scalable approaches to explore many interesting optoelectronic applications without the need of elaborate nanoscale patterning of graphene that could lead to significant damages to the graphene quality [238, 239]. Further research in developing PECVD techniques to synthesize VG-GNs with well controlled aspect ratios and absolute dimensions will be important to advance various applications based on VG-GNs.

5.2. Stacking order of multilayers

In our studies of horizontal growth of graphene sheets on copper foils by PECVD, we have found that the desirable number of layers can generally be controlled by the growth time under a given condition. On the other hand, our preliminary studies have revealed that the stacking order of graphene sheets is sensitively dependent on the specific growth parameters, particularly the partial pressures of CH_4, H_2 and N_2. As discussed in Section 2.1, the stacking order of multilayer graphene has important effects on the corresponding Raman spectroscopy. Additionally, the stacking order of graphene sheets plays an important role in determining the physical properties of graphene, including the formation of Moiré patterns that results in superlattice structures [240], potential modulations [241], and even the occurrence of unconventional superconductivity in bilayer graphene that is twisted at a magic angle [242]. Therefore, it is of both scientific and technological importance to explore reproducible and scalable synthesis techniques to control the stacking order in multilayer graphene. However, to date there have not been reports of systematic effort in controlling the stacking order of multilayer graphene. Further exploration of proper PECVD growth conditions to control both the number of graphene layers and the relative stacking order of consecutive graphene monolayers will likely open up new fronts of research for tuneable physical properties by simply controlling the relative angles of stacked graphene sheets.

5.3. Alignment of graphene nanostructures

It has been well recognized that spatially aligned one-dimensional (1D) nanostructures, such as CNTs, have significant advantages over randomly oriented 1D

nanostructure mats in various applications [10]. While we have demonstrated well aligned and densely packed MWCNT growth by MW-PECVD, as exemplified in Figures 4.5(c) and 4.5(f), the growth of GNSPs on copper generally yields random distributions in the long dimension, as shown in Figures 3.1(a) and 3.1(b). Such random distributions are likely related to the random seeding of precursor carbon radicals during the PECVD process, as schematically illustrated in Figure 3.2(a). Further development of growth methods to better align the long dimension of GNSPs, such as using templated substrates or better control of the gas flow direction during the PECVD growth process, will be desirable for optimizing the yield, aspect ratio and transferability (see next subsection) of the GNSPs.

5.4. Sample transfer technology

Although PECVD techniques have successfully grown graphene sheets and VG-GNs on a variety of substrates, not all materials are compatible with the PECVD growth process, nor can as-grown graphene and/or graphene nanostructures on the growth substrates be directly used for all applications. Therefore, it is important to develop proper transfer methods to remove graphene sheets and graphene nanostructures from their growth substrates to other desirable surfaces and/or devices while preserving the quality of the material. In the case of graphene sheets grown on metallic substrates, existing processes for transferring graphene from the growth substrates to other surfaces include three types of approaches: polymer-supported methods [243–246], polymer-free/water-assisted methods [247–249], and a polymer-free/water-free method [177]. While each approach has its specific strengths and shortcomings, all transfer methods involve chemical etching of the metallic substrates, which is environmentally undesirable. In contrast, VG-GNs can be easily scraped off their growth metallic substrates, liquid exfoliated and dispersed in a suitable solvent (*e.g.*, N-methyl-pyrrolidone [6]), and then centrifuged on desirable surfaces. All in all, there is still plenty of room for improvement in the transfer technology of graphene sheets and graphene-based nanostructures. More efforts are clearly needed in developing environmentally friendly and simpler methods for transferring PECVD-grown graphene from growth substrates to desirable surfaces without degrading the graphene quality.

6. Summary and outlook

We have reviewed recent progress in the synthesis of graphene and graphene-based nanostructures on a variety of substrates by means of PECVD techniques. The graphene synthesis includes horizontal growth of monolayer and multilayer graphene sheets, vertical growth of graphene nanostructures such as graphene nano-sheets and graphene nanostripes (GNSPs) with large aspect ratios, direct and selective deposition of monolayer and multilayer graphene on nanostructures, and vertical growth of multi-wall carbon nanotubes (MWCNTs). The rich chemical environment provided by PECVD enables graphene growth on a range of different material surfaces at lower temperatures and faster growth than typical thermal CVD growth. Additionally, proper choices of the precursor and source gases can simplify the graphene synthesis into a single-step process, provide control of the aspect ratios, and even induce desirable functionalities in the samples. Therefore, PECVD techniques for graphene synthesis are highly versatile and also promising for large-scale industrial applications.

On the other hand, a number of challenges remain. First, there has not been sufficient theoretical understanding for the complex growth environment of PECVD. More theoretical modelling together with systematic experimental investigation will certainly help the development of better parameters for graphene synthesis on different substrates by PECVD. Second, an important step towards industrial applications is to scale up the plasma sources and reaction chambers. Depending on the desirable size of the reaction chamber for specific applications, pulsed rather than continuous plasma sources may be required. The plasma environment for graphene synthesis may vary substantially from continuous to pulsed sources so that the optimized growth parameters may have to be modified. Finally, for practical purposes it is highly desirable to either directly deposit graphene on target surfaces without the need of transfer or develop simple and environmentally friendly methods to transfer graphene from the growth substrates to final targets. Although progress has been made in this aspect, more efforts are clearly needed to fully realize the potential of graphene based applications.

Acknowledgements

This work is jointly supported by the National Science Foundation, the Army Research Office, the Rothenberg Innovation Initiative Award at Caltech, and the Kavli Foundation.

References

[1] Novoselov K S *et al* 2005 Two-dimensional gas of massless Dirac fermions in graphene *Nature* **438** 197–200
[2] Geim A K *et al* 2007 The rise of graphene *Nat. Mater.* **6** 183–91
[3] Miao F *et al* 2007 Phase-coherent transport in graphene quantum billiards *Science* **317** 1530–1533
[4] Castro Neto A H *et al* 2009 The electronic properties of graphene *Rev. Mod. Phys.* **81** 109–162

[5] Blake P *et al* 2008 Graphene-based liquid crystal device *Nano Lett.* **8** 1704–1708
[6] Hernandez Y *et al* 2008 High-yield production of graphene by liquid-phase exfoliation of graphite *Nature Nanotechnol.* **3** 563–568
[7] Ohta T *et al* 2006 Controlling the electronic structure of bilayer graphene *Science* **313** 951–954
[8] Virojanadara C *et al* 2008 Homogeneous large-area graphene layer growth on 6*H*-SiC(0001) *Phys. Rev. B* **78** 245403
[9] Li X *et al* 2009 Large-area synthesis of high-quality and uniform graphene films on copper foils *Science* **324** 1312 - 1314
[10] Bo Z *et al* 2013 Plasma-enhanced chemical vapor deposition synthesis of vertically oriented graphene nanosheets *Nanoscale* **5** 5180–204
[11] Boyd D A *et al* 2015 Single-step deposition of high-mobility graphene at reduced temperatures *Nature Communications* **6**, 6620
[12] Hao Y *et al* 2013 The role of surface oxygen in the growth of large single-crystal graphene on copper *Science* **342** 720 - 723
[13] Yan Z *et al* 2012 Toward the synthesis of wafer-scale single-crystal graphene on copper foils *ACS Nano* **6** 9110
[14] Mun J H *et al* 2013 Synthesis of monolayer graphene Having a negligible amount of wrinkles by stress relaxation. *Nano Lett.* **13** 2496
[15] Liang T *et al* 2015 Graphene nucleation preferentially at oxygen-rich Cu sites rather than on pure Cu surface *Adv. Mater.* **27** 6404 –6410
[16] Liang T *et al* 2017 Exploring oxygen in graphene chemical vapor deposition synthesis *Nanoscale* **9** 3719 – 3735
[17] Habib M R *et al* 2018 A review of theoretical study of graphene chemical vapor deposition synthesis on metals: nucleation, growth, and the role of hydrogen and oxygen *Rep. Prog. Phys.* **81** 036501
[18] Wang S M *et al* 2013 A growth mechanism for graphene deposited on polycrystalline Co film by plasma enhanced chemical vapor deposition *New J. Chem.* **37** 1616
[19] Wang S M *et al* 2010 Synthesis of graphene on a polycrystalline Co film by radio-frequency plasma-enhanced chemical vapour deposition *J. Phys. D: Appl. Phys.* **43** 455402
[20] Woo Y *et al* 2009 Large-grained and highly-ordered graphene synthesized by radio frequency plasma-enhanced chemical vapor deposition *ECS Trans.* **19** 111.
[21] Nandamuri G *et al* 2010 Remote plasma assisted growth of graphene films *Appl. Phys. Lett.* **96** 154101.
[22] Kim Y *et al* 2011 Low-temperature synthesis of graphene on nickel foil by microwave plasma chemical vapor deposition *Appl. Phys. Lett.* **98** 263106.
[23] Peng K J *et al* 2013 Hydrogen-free PECVD growth of few-layer graphene on an ultra-thin nickel film at the threshold dissolution temperature *J. Mater. Chem. C* **1** 3862
[24] Kim J *et al* 2011 Low-temperature synthesis of large-area graphene-based transparent conductive films using surface wave plasma chemical vapor deposition *Appl. Phys. Lett.* **98** 091502
[25] Terasawa T *et al* 2012 Synthesis of nitrogen-doped graphene by plasma-enhanced chemical vapor deposition *Carbon* **50** 869.
[26] Yamada T *et al* 2013 Large area coating of graphene at low temperature using a roll-to-roll microwave plasma chemical vapor deposition *Thin Solid Films* **532** 89–93
[27] Kim Y S *et al* 2013 Methane as an effective hydrogen source for single-layer graphene synthesis on Cu foil by plasma enhanced chemical vapor deposition *Nanoscale* **5** 1221
[28] Kalita G *et al* 2012 Low temperature growth of graphene film by microwave assisted surface wave plasma CVD for transparent electrode application *RSC Advances* **2** 2815–2820
[29] Chan S H *et al* 2013 Low-temperature synthesis of graphene on Cu using plasma-assisted thermal chemical vapor deposition *Nanoscale Research Letters* **8** 285
[30] Nang L V *et al* 2012 Controllable synthesis of high-quality graphene using inductively-coupled plasma chemical vapor deposition *J. Electrochem. Soc.* **159** K93
[31] Laan T V D *et al* 2015 Water-mediated and instantaneous transfer of graphene grown at 220 °C enabled by a plasma *Nanoscale* 7 20564
[32] Malard L M *et al* 2009 Raman spectroscopy in graphene *Phys. Rep.* **473** 51-87
[33] Ferrari A C *et al* 2006 Raman spectrum of graphene and graphene layers *Phys. Rev. Lett.* **97** 187401
[34] Cancado L G *et al* 2006 General equation for the determination of the crystallite size La of nanographite by Raman spectroscopy *Appl. Phys. Lett.* **88** 163106
[35] Kahn A *et al* 2018 Direct CVD Growth of Graphene on Technologically Important Dielectric and Semiconducting Substrates *Adv. Sci.* **5** 1800050
[36] Wang H *et al* 2016 Direct CVD Graphene Growth on Semiconductors and Dielectrics for Transfer-Free Device Fabrication *Adv. Mater.* **28** 4956–4975
[37] Kiraly B *et al* 2015 Electronic and Mechanical Properties of Graphene-Germanium Interfaces Grown by Chemical Vapor Deposition *Nano Lett.* **15** 7414-7420
[38] Pasternak I *et al* 2016 Graphene growth on Ge(100)/Si(100) substrates by CVD method *Sci. Rep.* **6** 21773
[39] Pasternak I *et al* 2016 Large-area high-quality graphene on Ge(001)/Si(001) substrates *Nanoscale* **8** 11241-11247
[40] Dabrowski J *et al* 2016 Understanding the growth mechanism of graphene on Ge/Si(001) surfaces *Sci. Rep*. **6** 31639
[41] Takami T *et al* 2009 Catalyst-Free Growth of Networked Nanographite on Si and SiO2 Substrates by Photoemission-Assisted Plasma-Enhanced Chemical Vapor Deposition *e-J. Surf. Sci. Nanotechnol.* **7** 882-890
[42] Adhikari S *et al* 2016 Catalyst-Free Growth of Graphene by Microwave Surface Wave Plasma Chemical Vapor Deposition at Low Temperature *J. Mater. Sci. Chem. Eng*. **4** 10-14
[43] Zhou Q *et al* 2017 The controlled growth of graphene nanowalls on Si for Schottky photodetector *AIP Adv.* **7** 125317

[44] Zhang L *et al* 2011 Catalyst-free growth of nanographene films on various substrates *Nano Res.* **4** 315-321
[45] Sun J *et al* 2012 Direct Chemical Vapor Deposition of Large-Area Carbon Thin Films on Gallium Nitride for Transparent Electrodes: A First Attempt *IEEE Trans. Semicond. Manuf.* **25** 494-501
[46] Kim *et al* 2014 Direct integration of polycrystalline graphene into light emitting diodes by plasma-assisted metal-catalyst-free synthesis *ACS Nano* **8** 2230
[47] Ghosh S *et al* 2017 Process-specific mechanisms of vertically oriented graphene growth in plasmas *Nanotechnol* **8** 1658-1670
[48] Peng Z *et al* 2011 Direct growth of bilayer graphene on SiO_2 substrates by carbon diffusion through nickel *ACS Nano* **5** 8241-8247
[49] Wang D *et al* 2013 Scalable and direct growth of graphene micro ribbons on dielectric substrates *Sci. Rep*. **3** 1348
[50] Su C-Y *et al* 2011 Direct formation of wafer scale graphene thin layers on insulating substrates by chemical vapor deposition *Nano Lett*. **11** 3612-3216
[51] Kim H *et al* 2013 Copper-vapor-assisted chemical vapor deposition for high-quality and metal-free single-layer graphene on amorphous SiO2 substrate *ACS Nano* **7** 6575-6582
[52] Yang W *et al* 2013 Epitaxial growth of single-domain graphene on hexagonal boron nitride *Nat. Mater.* **12** 792
[53] Zhang L C *et al* 2011 Catalyst-free growth of nanographene films on various substrates *Nano Res.* **4** 315
[54] Yang W *et al* 2012 Growth, characterization, and properties of nanographene *Small* **8** 1429.
[55] Wei D *et al* 2013 Critical crystal growth of graphene on dielectric substrates at low temperature for electronic devices *Angew. Chem., Int. Ed.* **52** 14121
[56] Kato T *et al* 2012 Direct growth of doping-density-controlled hexagonal graphene on SiO_2 substrate by rapid-heating plasma CVD *ACS Nano* **6** 8508
[57] Dean C R *et al* 2013 Hofstadter's butterfly and the fractal quantum Hall effect in moiré superlattices *Nature* **497** 598
[58] Meng J H *et al* 2015 Synthesis of in-plane and stacked graphene/hexagonal boron nitride heterostructures by combining with ion beam sputtering deposition and chemical vapor deposition *Nanoscale* **7** 16046
[59] Dean C R *et al* 2010 Boron nitride substrates for high-quality graphene electronics *Nature Nanotech.* **5** 722-726
[60] Xue J M *et al* 2011 Scanning tunneling microscopy and spectroscopy of ultra-flat graphene on hexagonal boron nitride. *Nature Mater.* **10** 282285
[61] Hsu C-C *et al* 2018 High-yield single-step catalytic growth of graphene nanostripes by plasma enhanced chemical vapor deposition *Carbon* **129** 527–536
[62] Yeh N-C *et al* 2016 Nanoscale strain engineering of graphene and graphene-based devices *Acta Mech. Sin.* **32** 497 – 509
[63] Yeh N-C *et al* 2011 Strain-induced pseudomagnetic fields and charging effects on CVD-grown graphene *Surf. Sci.* **605** 1649–1656
[64] Levy N *et al* 2010 Strain-induced pseudomagnetic fields greater than 300 Tesla in graphene nanobubbles *Science* **329** 544
[65] Guinea F *et al* 2010 Energy gaps and a zerofield quantum Hall effect in graphene by strain engineering *Nat. Phys.* **6** 30–33
[66] Bunch J S *et al* 2008 Impermeable atomic membranes from graphene sheets *Nano Lett.* **8** 2458
[67] Chen S *et al* 2011 Oxidation resistance of graphene-coated Cu and Cu/Ni alloy *ACS Nano* **5** 1321
[68] Kang C G *et al* 2013 Effects of multi-layer graphene capping on Cu interconnects *Nanotechnology* **24** 115707.
[69] Mehta R *et al* 2015 Enhanced electrical and thermal conduction in graphene-encapsulated copper nanowires *Nano Lett.* **15** 2024–2030
[70] Mehta R *et al* 2017 Transfer-free multi-layer graphene as a diffusion barrier *Nanoscale* **9** 1827
[71] Jiang L *et al* 2013 Controlled synthesis of large-scale, uniform, vertically standing graphene for high-performance field emitters *Adv. Mater.* **25** 250–255
[72] Shuai X *et al* 2017 Wettability of vertically-oriented graphenes with different intersheet distances *RSC Adv.* **7** 2667–2675
[73] Qi J L *et al* 2016 Low resistance VFG-Microporous hybrid Al-based electrodes for supercapacitors *Nano Energy* **26** 657–67
[74] Zhang L X *et al* 2016 Understanding the growth mechanism of vertically aligned graphene and control of its wettability *Carbon* **103** 339–45
[75] Cuxart M G *et al* 2017 Inductively coupled remote plasma-enhanced chemical vapor deposition (rPE-CVD) as a versatile route for the deposition of graphene micro- and nanostructures *Carbon* **117** 331–42
[76] Kwon S H *et al* 2018 Structural and electrical characteristics of carbon nanowalls synthesized on the polyimide film *J Nanosci. Nanotechnol.* **18** 6309-6311
[77] Zheng S *et al* 2017 High packing density unidirectional arrays of vertically aligned graphene with enhanced areal capacitance for high-power micro-supercapacitors *ACS Nano* **11** 4009–16
[78] Amano T *et al* 2017 Rapid growth of micron-sized graphene flakes using in-liquid plasma employing iron phthalocyanine-added ethanol *Appl. Phys. Express* **11** 015102
[79] Russo P *et al* 2017 Carbon nanowalls: A new material for resistive switching memory devices *Carbon* **120** 54–62
[80] Liao Q *et al* 2015 All-solid-state symmetric supercapacitor based on Co_3O_4 nanoparticles on vertically aligned graphene *ACS Nano* **9** 5310–5317
[81] Yang H *et al* 2016 Edge effects in vertically-oriented graphene based electric double-layer capacitors *J. Power Sources* **324** 309–316
[82] Acik M *et al* 2011 Nature of graphene edges: A review *Jpn. J. Appl. Phys.* **50** 070101
[83] Bellunato A *et al* 2016 Chemistry at the edge of graphene *ChemPhysChem* **17** 785–801
[84] Premathilake D *et al* 2017 Electric double layer capacitors for ac filtering made from vertically oriented graphene nanosheets on aluminum *Carbon* **111** 231–237

[85] Hu L *et al* 2017 Direct anodic exfoliation of graphite onto high-density aligned graphene for large capacity supercapacitors *Nano Energy* **34** 515–523

[86] Li J *et al* 2016 Engineering micro-supercapacitors of graphene nanowalls/Ni heterostructure based on microfabrication technology *Appl. Phys. Lett.* **109** 153901

[87] Ghosh S *et al* 2017 Enhanced supercapacitance of activated vertical graphene nanosheets in hybrid electrolyte *J. Appl. Phys.* **122** 214902

[88] Premathilake D *et al* 2018 Fast response, carbon-black-coated, vertically-oriented graphene electric double layer capacitors *J. Electrochem. Soc.* **165** A924–931

[89] Xiong G *et al* 2016 Hierarchical Ni–Co Hydroxide Petals on Mechanically Robust Graphene Petal Foam for High-Energy Asymmetric Supercapacitors *Adv. Funct. Mater.* **26** 5460–5470

[90] Cheikh Z B *et al* 2017 Hydrogen doped $BaTiO_3$ films as solid-state electrolyte for micro-supercapacitor applications *J. Alloys Compd.* **721** 276–284

[91] Zhang Y *et al* 2016 Morphology Effect of Vertical Graphene on the High Performance of Supercapacitor Electrode *ACS Appl. Mater. Interfaces* **8** 7363–7369

[92] Chi Y-W *et al* 2016 New approach for high-voltage electrical double-layer capacitors using vertical graphene nanowalls with and without nitrogen doping *Nano Lett.* **16** 5719–27

[93] Wang M *et al* 2017 Nitrogen-doped graphene forests as electrodes for high-performance wearable supercapacitors *Electrochimica Acta* **250** 320–6

[94] Han Z J *et al* 2017 RuO_2 -coated vertical graphene hybrid electrodes for high-performance solid-state supercapacitors *J. Mater. Chem. A* **5** 17293–17301

[95] Sheng L *et al* 2017 Vertically oriented graphene nanoribbon fibers for high-volumetric energy density all-solid-state asymmetric supercapacitors *Small* **13** 1700371

[96] He P *et al* 2018 Vertically-oriented graphene nanosheet as nano-bridge for pseudocapacitive electrode with ultrahigh electrochemical stability *RSC Adv.* **8** 13891–13897

[97] Zhang Y J *et al* 2018 Composite Li metal anode with vertical graphene host for high performance Li-S batteries *J. Power Sources* **374** 205–210

[98] Zhan J *et al* 2018 Exploring hydrogen molybdenum bronze for sodium ion storage: Performance enhancement by vertical graphene core and conductive polymer shell *Nano Energy* **44** 265–271

[99] Mironovich V *et al* 2017 Gaining cycling stability of Si- and Ge-based negative Li-ion high areal capacity electrodes by using carbon nanowall scaffolds *J. Mater. Chem. A* **5** 18095–18100

[100] Li W *et al* 2015 Graphene-nanowall-decorated carbon felt with excellent electrochemical activity toward VO_2^+/VO_2^+ couple for all vanadium redox flow battery *Adv. Sci.* **3** 1500276

[101] Zheng Z *et al* 2016 High sulfur loading in hierarchical porous carbon rods constructed by vertically oriented porous graphene-like nanosheets for Li-S batteries *Adv. Funct. Mater.* **26** 8952–8959

[102] Yao Z *et al* 2017 Hybrid vertical graphene/lithium titanate–CNTs arrays for lithium ion storage with extraordinary performance *J. Mater. Chem. A* **5** 8916–8921

[103] Wu J *et al* 2016 Plasma-produced vertical carbonous nanoflakes for Li-ion batteries *Plasma Process. Polym.* **13** 1008–1014

[104] Su D *et al* 2016 Ruthenium nanocrystal decorated vertical graphene nanosheets@Ni foam as highly efficient cathode catalysts for lithium-oxygen batteries *NPG Asia Mater.* **8** e286

[105] Wang C *et al* 2017 Side-by-side observation of the interfacial improvement of vertical graphene-coated silicon nanocone anodes for lithium-ion batteries by patterning technology *Nanoscale* **9** 17241–17247

[106] Wang D *et al* 2017 Vertical-aligned Li_2S–graphene encapsulated within a carbon shell as a free-standing cathode for lithium–sulfur batteries *Chem. – Eur. J.* **23** 11169–11174

[107] Han C-P *et al* 2018 Vertically-aligned graphene nanowalls grown via plasma-enhanced chemical vapor deposition as a binder-free cathode in Li–O_2 batteries *Nanotechnology* **29**, 505401

[108] Ren H *et al* 2017 Hierarchical graphene foam for efficient omnidirectional solar–thermal energy conversion *Adv. Mater.* **29** 1702590

[109] Jiao T *et al* 2016 High-efficiency, stable and non-chemically doped graphene–Si solar cells through interface engineering and PMMA antireflection *RSC Adv.* **6** 10175–10179

[110] Jung Y H *et al* 2016 Properties of dye-sensitized solar cells using carbon nanowall counter electrodes *J Nanosci. Nanotechnol.* **16** 5302-5304

[111] Wei W *et al* 2017 Synthesis of mesochannel carbon nanowall material from CO_2 and its excellent performance for perovskite solar cells *Ind. Eng. Chem. Res.* **56** 1803–1809

[112] Zhou Q *et al* 2017 The controlled growth of graphene nanowalls on Si for Schottky photodetector *AIP Adv.* **7** 125317

[113] Zhou Q *et al* 2018 The interface modification for GNWs/Si Schottky junction with PEI/PEIE interlayers *Mater. Res. Express* **5** 035605

[114] Miao F *et al* 2017 Vertically-oriented few-layer graphene supported by silicon microchannel plates as a counter electrode in dye-sensitized solar cells *Org. Electron.* **45** 74–80

[115] Lin G *et al* 2017 Direct growth of graphene nanowalls on quartz substrates as transparent conductive electrodes for perovskite solar cells *Funct. Mater. Lett.* **11** 1850009

[116] Lehmann K *et al* 2018 High electrocatalytic activity of metal-free and non-doped hierarchical carbon nanowalls towards oxygen reduction reaction *Electrochimica Acta* **269** 657–67

[117] Imai S *et al* 2017 High-durability catalytic electrode composed of Pt nanoparticle-supported carbon nanowalls synthesized by radical-injection plasma-enhanced chemical vapor deposition *J. Phys. Appl. Phys.* **50** 40LT01

[118] Höltig M *et al* 2016 Highly efficient fuel cell electrodes from few-layer graphene sheets and electrochemically

deposited palladium nanoparticles *J. Phys. Chem. C* **120** 7476–7481

[119] Zhang H *et al* 2017 Pt decorated 3D vertical graphene nanosheet arrays for efficient methanol oxidation and hydrogen evolution reactions *J. Mater. Chem. A* **5** 22004–22011

[120] Akbar K *et al* 2017 Superaerophobic graphene nano-hills for direct hydrazine fuel cells *NPG Asia Mater.* **9** e378

[121] Lu C *et al* 2016 Characteristic study of boron doped carbon nanowalls films deposited by microwave plasma enhanced chemical vapor deposition *J Nanosci Nanotechnol.* **16** 1680

[122] Chi Y *et al* 2016 Directly deposited graphene nanowalls on carbon fiber for improving the interface strength in composites *Appl. Phys. Lett.* **108** 211601

[123] Cheng L *et al* 2016 High-efficiency field emission from pressed nickel foam–flat graphene–vertical graphene hybrids *Mater. Lett.* **176** 165–8

[124] Deng J-H *et al* 2017 Highly improved field emission from vertical graphene–carbon nanotube composites *J. Alloys Compd.* **723** 75–83

[125] Belyanin A F *et al* 2017 On the effect of laser irradiation and heat treatment on the structure and field-emission properties of carbon nanowalls *J. Surf. Investig. X-Ray Synchrotron Neutron Tech.* **11** 295–304

[126] Zhao C X *et al* 2016 Surface nitrogen functionality for the enhanced field emission of free-standing few-layer graphene nanowalls *J. Alloys Compd.* **672** 433–439

[127] Tian F *et al* 2017 A tantalum electrode coated with graphene nanowalls for simultaneous voltammetric determination of dopamine, uric acid, L-tyrosine, and hydrochlorothiazide *Microchim. Acta* **184** 1611–1619

[128] S. Hosu *et al* 2017 Carbon nanowalls: a new versatile graphene based interface for the laser desorption/ionization-mass spectrometry detection of small compounds in real samples *Nanoscale* **9** 9701–9715

[129] Dyakonov P *et al* 2017 Carbon nanowalls as a platform for biological SERS studies *Sci. Rep.* **7** 13352

[130] Bo Z *et al* 2018 Decoration of vertical graphene with tin dioxide nanoparticles for highly sensitive room temperature formaldehyde sensing *Sens. Actuators B Chem.* **256** 1011–1020

[131] Kawahara T *et al* 2016 Development of nano-carbon biosensors using glycan for host range detection of influenza virus *Condens. Matter* **1** 7

[132] Wu Y *et al* 2017 Direct electrodeposition to fabricate vertically-oriented graphene nanosheets modified electrode and its application for determination of levodopa in the presence of uric acid and ascorbic acid *Nano* **12** 1750087

[133] Chen Q *et al* 2017 Flexible electrochemical biosensors based on graphene nanowalls for the real-time measurement of lactate *Nanotechnology* **28** 315501

[134] Tzouvadaki I *et al* 2018 Graphene nanowalls for high-performance chemotherapeutic drug sensing and anti-fouling properties *Sens. Actuators B Chem.* **262** 395–403

[135] Tomatsu M *et al* 2017 Hydrogen peroxide sensor based on carbon nanowalls grown by plasma-enhanced chemical vapor deposition *Jpn. J. Appl. Phys.* **56** 06HF03

[136] Gao D *et al* 2017 Sensitive detection of biomolecules and DNA bases based on graphene nanosheets *J. Solid State Electrochem.* **21** 813–821

[137] Pandit S *et al* 2018 Vertically aligned graphene coating is bactericidal and prevents the formation of bacterial biofilms *Adv. Mater. Interfaces* **5** 1701331

[138] Lee J-H *et al* 2016 CMOS-compatible catalytic growth of graphene on a silicon dioxide substrate *Appl. Phys. Lett.* **109** 053102

[139] Komarova N *et al* 2017 Redox reactions of $[Ru(NH_3)_6]^{2+/3+}$, $[Fe(CN)_6]^{3-/4-}$ and $Fe^{2+/3+}$ on pristine and electrochemically modified carbon nanowalls under physical adsorption of compounds with the skeletal and macrocyclic structure *J. Electroanal. Chem.* **788** 1–6

[140] Zhang Y *et al* 2018 Enhanced magnetoimpedance effect of $Fe_{75.5}Cu_1Nb_3Si_{13.5}B_7$ ribbon covered by in-situ growth vertical graphene sheets *Mater. Lett.* **222** 131–134

[141] Borghi F F *et al* 2018 Nanostructured graphene surfaces promote different stages of bone cell eifferentiation *Nano-Micro Lett.* **10** 47

[142] Ion R *et al* 2016 Vertically, interconnected carbon nanowalls as biocompatible scaffolds for osteoblast cells *J. Phys. Appl. Phys.* **49** 274004

[143] Zhang Y-F *et al* 2018 Vertically aligned graphene film/epoxy composites as heat dissipating materials *Int. J. Heat Mass Transf.* **118** 510–7

[144] Sun Z *et al* 2017 Effect of vertically oriented few-layer graphene on the wettability and interfacial reactions of the AgCuTi-SiO_{2f} /SiO_2 system *Sci. Rep.* **7** 224

[145] Li M *et al* 2016 Controllable synthesis of graphene by plasma-enhanced chemical vapor deposition and its related applications *Adv. Sci.* **3** n/a-n/a

[146] Chen L *et al* 2017 Graphene field emitters: A review of fabrication, characterization and properties *Mater. Sci. Eng. B* **220** 44–458

[147] Ashraf A *et al* 2014 Spectroscopic investigation of the wettability of multilayer graphene using highly ordered pyrolytic graphite as a model material *Langmuir* **30** 12827-1283

[148] Khan A *et al* 2018 Wetting behaviors and applications of metal-catalyzed CVD grown graphene *J. Mater. Chem. A* **6** 22437-22464

[149] Hassouni K *et al* 2010 Modelling of diamond deposition microwave cavity generated plasmas *J. Phys. Appl. Phys.* **43** 153001

[150] Lehmann K *et al* 2016 Effect of the aromatic precursor flow rate on the morphology and properties of carbon nanostructures in plasma enhanced chemical vapor deposition *RSC Adv.* **6** 32779–32788

[151] Ouyang B *et al* 2016 Green synthesis of vertical graphene nanosheets and their application in high-performance supercapacitors *RSC Adv.* **6** 23968–23973

[152] Seo D H *et al* 2013 Structure-controlled vertical graphene-based, binder-free electrodes from plasma-reformed butter enhance supercapacitor performance *Adv. Energy Mater.* **3** 1316–1323

[153] Wu A *et al* 2017 Upcycling waste lard oil into vertical graphene sheets by inductively coupled plasma assisted chemical vapor deposition *Nanomaterials* **7** 318

[154] Prasad K *et al* 2017 Effect of precursor on antifouling efficacy of vertically-oriented graphene nanosheets *Nanomaterials* **7** 170

[155] Zhou L *et al* 2017 Facile syntheses of 3-dimension graphene aerogel and nanowalls with high specific surface areas *Chem. Phys. Lett.* **677** 7–12

[156] Garg R *et al* 2017 Nanowire-mesh-templated growth of out-of-plane three-dimensional fuzzy graphene *ACS Nano* **11** 6301–6311

[157] Hu C *et al* 2018 Functionalization of graphene materials by heteroatom-doping for energy conversion and storage *Prog. Nat. Sci. Mater. Int.* **28** 121–132

[158] Wang X *et al* 2014 Heteroatom-doped graphene materials: syntheses, properties and applications *Chem. Soc. Rev.* **43** 7067–7098

[159] Soin N *et al* 2011 Enhanced and stable field emission from in situ nitrogen-doped few-layered graphene nanoflakes *J. Phys. Chem. C* **115** 5366–5372

[160] Sobaszek M *et al* 2017 Diamond phase (sp^3-C) rich boron-doped carbon nanowalls (sp^2-C): Physicochemical and electrochemical properties *J. Phys. Chem. C* **121** 20821–20833

[161] Siuzdak K *et al* 2017 Boron-enhanced growth of micron-scale carbon-based nanowalls: A route toward high rates of electrochemical biosensing *ACS Appl. Mater. Interfaces* **9** 12982–12992

[162] Satulu V *et al* 2016 Plasma processing with fluorine chemistry for modification of surfaces wettability *Molecules* **21** 1711

[163] Davami K *et al* 2016 Modification of mechanical properties of vertical graphene sheets via fluorination *RSC Adv.* **6** 11161–11166

[164] Lin C *et al* 2017 Enhancing the stiffness of vertical graphene sheets through ion beam irradiation and fluorination *Nanotechnology* **28** 295701

[165] Ghosh S *et al* 2018 Influence of nitrogen on the growth of vertical graphene nanosheets under plasma *J. Mater. Sci.* **53** 7316–7325

[166] Suetin V *et al* 2016 Self-assembled nanoparticle patterns on carbon nanowall surfaces *Phys. Chem. Chem. Phys.* **18** 12344–12349

[167] Ren W *et al* 2017 Ultrathin MoS_2 nanosheets@metal organic framework-derived n-doped carbon nanowall arrays as sodium ion battery anode with superior cycling life and rate capability *Adv. Funct. Mater.* **27** 1702116

[168] Ouyang B *et al* 2016 MoS_2 anchored free-standing three dimensional vertical graphene foam based binder-free electrodes for enhanced lithium-ion storage *Electrochimica Acta* **194** 151–160

[169] Khanis N H *et al* 2017 SnO_2 Nanoparticles Decorated 2D Wavy Hierarchical Carbon Nanowalls with Enhanced Photoelectrochemical Performance *J. Nanomater.* **2017** 4315905

[170] Davami K *et al* 2016 Tuning the mechanical properties of vertical graphene sheets through atomic layer deposition *Nanotechnology* **27** 155701

[171] Park J K *et al* 2018 Improvement of electrical properties of carbon nanowall by the deposition of thin film *J Nanosci Nanotechnol.* **18** 6026

[172] Wu J-B *et al* 2018 Raman spectroscopy of graphene-based materials and its applications in related devices *Chem. Soc. Rev.* **47** 1822–73

[173] Ghosh S *et al* 2018 Plasma-electric field controlled growth of oriented graphene for energy storage applications *J. Phys. Appl. Phys.* **51** 145303

[174] Meyer J C *et al* 2007 On the roughness of single- and bi-layer graphene membranes *Solid State Commun.* **143** 101–109

[175] Ganesan K *et al* 2016 A comparative study on defect estimation using XPS and Raman spectroscopy in few layer nanographitic structures *Phys. Chem. Chem. Phys.* **18** 22160–22167

[176] Kim H *et al* 2014 Organic solar cells using CVD-grown graphene electrodes *Nanotechnology* **25**, 014012

[177] Tseng W-H *et al* 2017 Stabilization of hybrid perovskite $CH_3NH_3PbI_3$ thin films by graphene passivation *Nanoscale* **9** 19227—19235

[178] Hsu H-C *et al* 2012 Stand-up structure of graphene-like carbon nanowalls on CNT directly grown on polyacrylonitrile-based carbon fiber paper as supercapacitor *Diam. Relat. Mater.* **25** 176–9

[179] Zhao R *et al* 2017 Electrical transport properties of graphene nanowalls grown at low temperature using plasma enhanced chemical vapor deposition *Mater. Res. Express* **4** 055007

[180] Kumar P 2017 Temperature-dependent conduction mechanism of vertically aligned graphene nanoflakes incorporated with nitrogen in situ *Mater. Res. Express* **4** 075011

[181] Ghosh S *et al* 2018 Aging effects on vertical graphene nanosheets and their thermal stability *Indian J. Phys.* **92** 337–342

[182] Vizireanu S *et al* 2017 Aging phenomena and wettability control of plasma deposited carbon nanowall layers *Plasma Process. Polym.* **14** 1700023

[183] Mishra K K *et al* 2016 Thermal conductivity and pressure-dependent Raman studies of vertical graphene nanosheets *J. Phys. Chem. C* **120** 25092–100

[184] Dresselhaus M S *et al* 2005 Raman spectroscopy of carbon nanotubes *Phys. Rep.* **409** 47–99

[185] Lekawa-Raus A *et al* 2014 Electrical properties of carbon nanotube based fibers and their future use in electrical wiring *Adv. Funct. Mater.* **24** 3661

[186] Ebbesen T *et al* 1992 Large-scale synthesis of carbon nanotubes *Nature* **358** 220

[187] Smalley R *et al* 1998 One-dimensional nanostructures: Chemistry, physics & applications *Solid State Commun.* **11** 107

[188] Collins P *et al* 2000 Nanotubes for electronics *Sci. Am.* **283** 62

[189] Yu G *et al* 1995 Polymer photovoltaic cells: Enhanced efficiencies via a network of internal donor-acceptor heterojunctions *Science* **270** 1789

[190] Kymakis E *et al* 2002 Single-wall carbon nanotube/conjugated polymer photovoltaic devices *Appl. Phys. Lett.* **80** 112

[191] Yu D *et al* 2010 Soluble P3HT-grafted graphene for

efficient bilayer−heterojunction photovoltaic devices *ACS Nano* **4** 5633

[192] Liu Z *et al* 2002 Preparation and characterization of platinum-based electrocatalysts on multiwalled carbon nanotubes for proton exchange membrane fuel cells *Langmuir* **18** 4054

[193] Yu D *et al* 2010 Metal-free carbon nanomaterials become more active than metal catalysts and last longer *J. Phys. Chem. Lett.* **1** 2165.

[194] Welna D *et al* 2010 Vertically aligned carbon nanotube electrodes for lithium-ion batteries *J. Power Sources* **196** 1455

[195] Gogotsi Y *et al* 2011 True performance metrics in electrochemical energy storage *Science* **334** 917

[196] Izadi-Najafabadi A *et al* 2010 Extracting the full potential of single-walled carbon nanotubes as durable supercapacitor electrodes operable at 4 V with high power and energy density *Adv. Mater.* **22** E235.

[197] Rahaman M *et al* 2012 Electrochemical carbon-nanotube filter performance toward virus removal and inactivation in the presence of natural organic matter. *Environ. Sci. Technol.* **46** 1556

[198] Snow E *et al* 2005 Chemical detection with a single-walled carbon nanotube capacitor *Science* **307** 1942

[199] Esser B *et al* 2012 Selective detection of ethylene gas using carbon nanotube-based devices: utility in determination of fruit ripeness. *Angew. Chem. Int. Ed.* **51** 5752.

[200] Wilson M *et al* 2002 Nanotechnology: Basic science and emerging technologies CRC Press New York.

[201] Azami T *et al* 2007 Production of small single-wall carbon nanohorns by CO_2 laser ablation of graphite in Ne-gas atmosphere *Carbon* **45** 1364.

[202] Patole S *et al* 2008 Water-assisted synthesis of carbon nanotubes: Acetylene partial pressure and height control *EPL* **81** 6

[203] Huang L *et al* 2006 Cobalt ultrathin film catalyzed ethanol chemical vapor deposition of single-walled carbon nanotubes *J Phys Chem B* **110** 11103

[204] Zheng B *et al* 2002 Efficient CVD growth of single-walled carbon nanotubes on surfaces using carbon monoxide precursor *Nano Lett.* **2** 895

[205] Hata K *et al* 2004 Water-assisted highly efficient synthesis of impurity-free single-walled carbon nanotubes *Science* **306** 1362.

[206] Yang Q *et al* 2003 Direct growth of macroscopic fibers composed of large diameter SWNTs by CVD *Chem. Phys. Lett.* **370** 274

[207] Benito A *et al* 1998 Carbon nanotubes production by catalytic pyrolysis of benzene *Carbon* **36** 681

[208] Okada T *et al* 2007 Conversion of toluene into carbon nanotubes using arc discharge plasmas in solution *Thin Solid Films* **515** 4262

[209] José-Yacamán M *et al* 1993 Catalytic growth of carbon microtubules with fullerene structure *Appl. Phys. Lett.* **62** 657

[210] Maruyama S *et al* 2002 Low-temperature synthesis of high-purity single-walled carbon nanotubes from alcohol *Chemical Physics Letters* **360** 220

[211] Hata K *et al* 2004 Water-assisted highly efficient synthesis of impurity-free single-walled carbon nanotubes *Science* **306** 1362

[212] Zhao J *et al* 2011 Growth of carbon nanotubes on natural organic precursors by chemical vapor deposition *Carbon* **49** 2155

[213] Ding F *et al* 2008 The importance of strong carbon-metal adhesion for catalytic nucleation of single-walled carbon nanotubes *Nano Lett.* **8** 463

[214] Lee J *et al* 2001 Growth of carbon nanotubes on anodic aluminum oxide templates: Fabrication of a tube-in-tube and linearly joined tube *Chem. Mater.* **13** 2387

[215] Takagi D *et al* 2008 Mechanism of gold-catalyzed carbon material growth *Nano Lett.* **8** 832

[216] Zhou W *et al* 2006 Copper catalyzing growth of single-walled carbon nanotubes on substrates *Nano Lett*. **6** 2987

[217] Fan J *et al* 1999 Synthesis, characterizations, and physical properties of carbon nanotubes coated by conducting polypyrrole J. Appl. Polymer. Phys. **74** 2605

[218] Lobiaka E *et al* 2015 Ni–Mo and Co–Mo alloy nanoparticles for catalytic chemical vapor deposition synthesis of carbon nanotubes *J. Alloys and Compounds* **621** 351

[219] Takagi D *et al* 2009 Carbon nanotube growth from diamond *J. Am. Chem. Soc.* **131** 6922

[220] Rümmeli M *et al* 2005 Novel catalysts, room temperature, and the importance of oxygen for the synthesis of single-walled carbon nanotubes *Nano Lett.* **5** 1209

[221] Zhang R *et al* 2017 Horizontally aligned carbon nanotube arrays: growth mechanism, controlled synthesis, characterization, properties and applications *Chem. Soc. Rev.* **46** 3661-3715

[222] Kar R 2016 Detailed investigation on the mechanism of co-deposition of different carbon nanostructures by microwave plasma CVD Carbon 106 233.

[223] Gentoiu M A 2017 Morphology, Microstructure, and Hydrogen Content of Carbon Nanostructures Obtained by PECVD at Various Temperatures *Journal of Nanomaterials* **2017** 1

[224] Liu Y 2017 Confirming the key role of Ar+ ion bombardment in the growth feature of nanostructured carbon materials by PECVD *Nanotechnology* **28** 475601

[225] Patil V *et al* 2014 Graphene oxide and functionalized multi walled carbon nanotubes as epoxy curing agents: a novel synthetic approach to nanocomposites containing active nanostructured fillers *RSC Advances* **4** 49264

[226] Liu B *et al* 2011 Importance of Oxygen in the Metal-Free Catalytic Growth of Single-Walled Carbon Nanotubes from SiO_x by a Vapor-Solid-Solid Mechanism *J. Am. Chem. Soc.* **133** 197-199

[227] Zhang G *et al* 2005 Ultra-high-yield growth of vertical single-walled carbon nanotubes: Hidden roles of hydrogen and oxygen *Proc. Natl. Acad. Sci.* **102** 16141-16145

[228] Nair R R *et al* 2008 Fine structure constant defines visual transparency of graphene *Science* **320** 1308

[229] Kuzmenko A B *et al* 2008 Universal optical conductance of graphite. *Phys. Rev. Lett.* **100,** 117401

[230] Walavalkar S S *et al* 2010 Tunable visible and near-IR

emission from sub-10 nm etched single-crystal Si Nanopillars *Nano Lett.* **10** 4423–4428

[231] Zheng C *et al* 2013 Polarity-driven 3-fold symmetry of GaAs/AlGaAs core multishell nanowires *Nano Lett.* **13** 3742

[232] Fickenscher M *et al* 2013 Optical, structural, and numerical investigations of GaAs/AlGaAs core−multishell nanowire quantum well tubes *Nano Lett.* **13** 1016

[233] Shi T *et al* 2015 Emergence of localized states in narrow GaAs/AlGaAs nanowire quantum well tubes *Nano Lett.* **15** 1876

[234] Han M Y *et al* 2007 Energy band-gap engineering of graphene nanoribbons *Phys. Rev. Lett.* **98** 206805

[235] Lee E J H *et al* 2008 Contact and edge effects in graphene devices. *Nat. Nanotechnol.* **3,** 486–490

[236] Xia F N *et al* 2009 Ultrafast graphene photodetector. *Nat. Nanotechnol.* **4,** 839–843

[237] Mueller T *et al* 2010 Graphene photodetectors for high-speed optical communications. *Nat. Photonics* **4** 297–301

[238] Kim Y D *et al* 2015 Bright visible light emission from graphene *Nat. Nanotech.* **10** 676–682

[239] Senkovskiy B V *et al* 2017 Making graphene nanoribbons photoluminescent *Nano Lett.* **17** 4029−4037

[240] Bistritzer R *et al* 2011 Moiré bands in twisted double-layer graphene *PNAS* **108** 12233-12237

[241] Li G *et al* 2010 Observation of Van Hove singularities in twisted graphene layers *Nature Physics* **6** 109–113

[242] Cao Y *et al* 2018 Unconventional superconductivity in magic-angle graphene superlattices *Nature* **556** 43–50

[243] Li X *et al* 2009 Transfer of large-area graphene films for high-performance transparent conductive electrodes *Nano Lett.* **9** 4359–4363

[244] Kim K S *et al* 2009 Large-scale pattern growth of graphene films for stretchable transparent electrodes *Nature* **457** 706–710

[245] Lee W H *et al* 2012 Simultaneous transfer and doping of CVD-grown graphene by fluoropolymer for transparent conductive films on plastic *ACS Nano* **6** 1284–1290

[246] Gao L *et al* 2014 Face-to-face transfer of wafer-scale graphene films *Nature* **505** 190–194

[247] Wang D-Y *et al* 2013 Clean-lifting transfer of large-area residual-free graphene films *Adv. Mater.* **25** 4521–4526

[248] Jung W *et al* 2014 Ultraconformal contact transfer of monolayer graphene on metal to various substrates *Adv. Mater.* **26** 6394–6400

[249] Lin W-H *et al* 2014 A direct and polymer-free method for transferring graphene grown by chemical vapor deposition to any substrate *ACS Nano* **8** 1784–1791